USGS
science for a changing world

Post-Miocene Right Separation on the San Gabriel and Vasquez Creek Faults, with Supporting Chronostratigraphy, Western San Gabriel Mountains, California

Professional Paper 1759

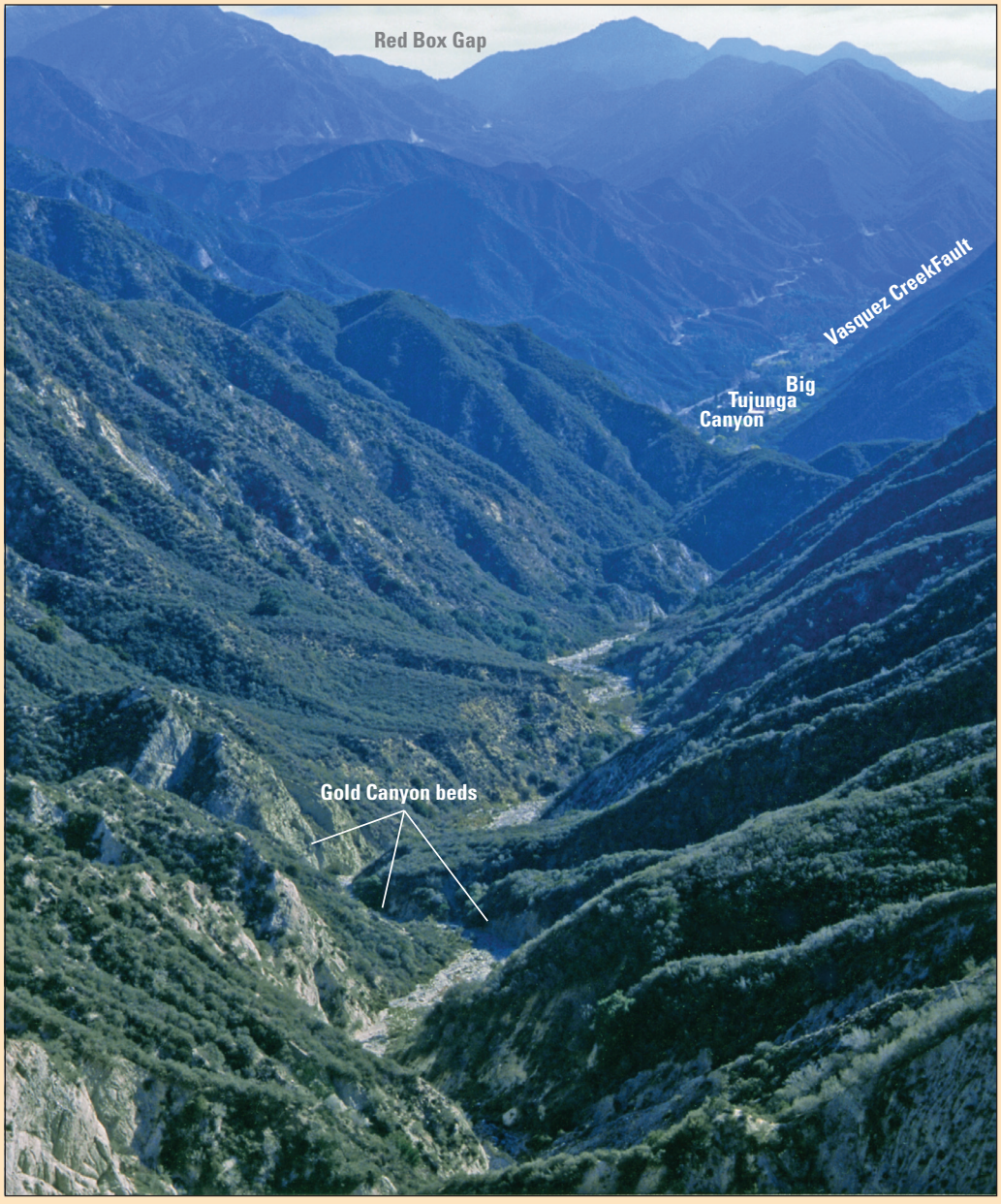

U.S. Department of the Interior
U.S. Geological Survey

FRONT COVER

View southeastward down Gold Canyon and (in distance) up part of Big Tujunga Canyon in the southwestern San Gabriel Mountains, southern California. Both canyons parallel the strike of the San Gabriel Fault Zone, which cuts their lower northeast (left) walls. At the bottom of Big Tujunga Canyon, the fault zone bifurcates—the north branch strikes to the east through Red Box Gap, and the south branch, the Vasquez Creek Fault, strikes to the southeast. In the bottom of Gold Canyon are outcrops of fossiliferous nearshore shallow marine sandstone of earliest Pliocene age, designated the Gold Canyon beds, overlain on the northeast (left) by steeply dipping Pliocene-Pleistocene fanglomerate. Both units are truncated by the fault zone at the base of the steep slope to the left. Distinctive clasts within the Gold Canyon beds, which can be matched to a clast source unit on the other side of the San Gabriel-Vasquez Creek Fault Zone, imply about 12 km of post-Miocene right separation on the zone. See figures 1 and 2 for location. USGS photograph by L.A. Beyer.

Post-Miocene Right Separation on the San Gabriel and Vasquez Creek Faults, with Supporting Chronostratigraphy, Western San Gabriel Mountains, California

By Larry A. Beyer, Thane H. McCulloh, Rodger E. Denison, Ronald W. Morin, Roy J. Enrico, John A. Barron, and Robert J. Fleck

Professional Paper 1759

U.S. Department of the Interior
U.S. Geological Survey

U.S. Department of the Interior
KEN SALAZAR, Secretary

U.S. Geological Survey
Suzette M. Kimball, Acting Director

U.S. Geological Survey, Reston, Virginia: 2009

This report and any updates to it are available online
at: http://pubs.usgs.gov/pp/1759/

For product and ordering information:
World Wide Web: http://www.usgs.gov/pubprod
Telephone: 1-888-ASK-USGS (1-888-275-8747)

For more information on the USGS—the Federal source for science about the Earth,
its natural and living resources, natural hazards, and the environment:
World Wide Web: http://www.usgs.gov
Telephone: 1-888-ASK-USGS

Suggested citation:
Beyer, L.A., McCulloh, T.H., Denison, R.E., Morin, R.W., Enrico, R.J., Barron, J.A., and Fleck, R.J., 2009, Post-Miocene right separation on the San Gabriel and Vasquez Creek Faults, with supporting chronostratigraphy, western San Gabriel Mountains, California: U.S. Geological Survey Professional Paper 1759, 44 p.

Cataloging-in-publication data are on file with the Library of Congress (http://www.loc.gov/)

Contents

Abstract 1
Introduction 1
Geologic Setting 3
Pre-Neogene Rocks 3
Neogene Stratigraphy and Chronostratigraphic Findings 3
    Volcanic Rocks of the Topanga Group 3
    Modelo Formation 3
    Towsley Formation 8
    Pico Formation 8
    Saugus Formation 8
    Chronostratigraphy: Ancilliary Paleogeographic and Strucutral Implications 9
Gold Canyon Beds 10
    Possible Correlative Strata 10
Right Separation on the Vasquez Creek Fault 14
    Probable Source of Mount Lowe Intrusive Suite Clasts in the Gold Canyon Beds: Constraint on Vasquez Creek Fault Displacement 14
    Saugus Formation Clasts, Probable Cross-Fault Sources, and Relevant Perspectives 16
        Local Tectonic Block Rotation 16
        Clast Size, Bed-Forming Process, and Distribution of Mount Lowe Clasts 17
        Fault Truncation of Clast Lithofacies Boundary 17
        Relative Abundances of Clast Types 17
        Summary 19
Conclusions 19
Acknowledgments 22
References 22

Appendixes

1. Description of Saugus Formation Clasts 30
2. Isotopic Age Determinations Using $^{87}Sr/^{86}Sr$ Ratio 34
3. Identification, Age, and Paleoenvironment of Calcareous Nannofossils 38
4. Identification, Age, and Paleoenvironment of Foraminifers and Occurrences of Fossil Oyster Spat 40
5. Identification and Zonation of Diatoms 42
6. Age of Basalt by $^{40}Ar/^{39}Ar$ Incremental-Heating Analysis 43

Figures

1. Principal geographic features and simplified fault map of San Gabriel Mountains and surrounding parts of southern California 2
2. Geologic maps of the southwestern San Gabriel Mountains and adjacent area to the west, California 4
3. Columnar sections of middle Miocene through middle Pleistocene strata showing inferred correlations from west of San Fernando Pass to mouth of Big Tujunga Canyon....6
4. Chronostratigraphic correlation diagram of middle Miocene through middle Pleistocene formations of the Merrick Syncline-Gold Canyon and San Fernando Pass areas....7
5. Local geologic map of Gold Canyon beds and upper Gold Canyon....9
6. Photographs of macrofossiliferous sandstone and polymitic breccia-conglomerate lens of the Gold Canyon beds....11
7. Simplified geologic map of the central and western San Gabriel Mountains emphasizing outcrops of Mount Lowe intrusive suite, anorthosite-syenite complex, and Paleoproterozoic gneiss suite, and faults....15
8. Map showing "Merrick Syncline domain" local tectonic block and hypothetical points of block rotation about vertical axes 17
9. Photographs of Saugus Formation fanglomerate in upper Gold Canyon 18
10. Maps showing distribution of maximum clast sizes and bed-forming processes of the Saugus Formation. 20
11. $^{40}Ar/^{39}Ar$ age spectrum and isochron diagrams for Topanga Group basalt sample from near mouth of Big Tujunga Canyon....43

Tables

1. Estimates of amount and timing of right separation on the Vasquez Creek Fault from published sources and this study....12
2. Maximum size, shape, and relative abundance of Saugus clasts derived from the Mount Lowe intrusive suite and anorthosite-syenite complex, at 63 localities from Pacoima Wash to Gold Canyon... 30
3. Analytical results and derived $^{87}Sr/^{86}Sr$ ages of Neogene fossil samples at 15 localities along the southwestern margin of the San Gabriel Mountains and in the San Fernando Pass area. 34
4. Abundance and CN zone range of identified calcareous nannofossils in Modelo Formation samples at three localities from Little Tujunga Canyon to near mouth of Big Tujunga Canyon....38
5. Abundance, zone range, and suggested paleoenvironment of identified foraminifers in Modelo Formation samples at four localities from Little Tujunga Canyon to near mouth of Big Tujunga Canyon 40
6. Abundance and zone range of identified diatoms in Modelo Formation samples from two localities near mouth of Big Tujunga Canyon....42
7. Results of $^{40}Ar/^{39}Ar$ age analysis of Topanga Group basalt sample from locality near mouth of Big Tujunga Canyon 44

Post-Miocene Right Separation on the San Gabriel and Vasquez Creek Faults, with Supporting Chronostratigraphy, Western San Gabriel Mountains, California

By Larry A. Beyer[1] , Thane H. McCulloh[2] , Rodger E. Denison[3] , Ronald W. Morin[4] , Roy J. Enrico[5] , John A. Barron[1], and Robert J. Fleck[1]

Abstract

The right lateral San Gabriel Fault Zone in southern California extends from the northwestern corner of the Ridge Basin southeastward to the eastern end of the San Gabriel Mountains. It bifurcates to the southeast in the northwestern San Gabriel Mountains. The northern and older branch curves eastward in the range interior. The southern younger branch, the Vasquez Creek Fault, curves southeastward to merge with the Sierra Madre Fault Zone, which separates the San Gabriel Mountains from the northern Los Angeles Basin margin. An isolated exposure of partly macrofossiliferous nearshore shallow-marine sandstone, designated the Gold Canyon beds, is part of the southwest wall of the fault zone 5.5 km northwest of the bifurcation. These beds contain multiple subordinate breccia-conglomerate lenses and are overlain unconformably by folded Pliocene-Pleistocene Saugus Formation fanglomerate. The San Gabriel Fault Zone cuts both units.

Marine macrofossils from the Gold Canyon beds give an age of 5.2±0.3 Ma by $^{87}Sr/^{86}Sr$ analyses. Magnetic polarity stratigraphy dates deposition of the overlying Saugus Formation to between 2.6 Ma and 0.78 Ma (Levi and Yeats, 2003). Distinctive metaplutonic rocks of the Mount Lowe intrusive suite (of Morton and Miller, 2003; Barth and Ehlig, 1988) in the San Gabriel Range are the source of certain clasts in both the Gold Canyon beds and Saugus Formation. Angular clasts of nondurable Paleocene sandstone also occur in the Gold Canyon beds. The large size and angularity of some of the largest of both clast types in breccia-conglomerate lenses of the beds suggest landslides or debris flows from steep terrain. Sources of Mount Lowe clasts, originally to the north or northeast, are now displaced southeastward by faulting and are located between the San Gabriel and Vasquez Creek faults, indicating as much as 12±2 km of post-Miocene Vasquez Creek Fault right separation, in accord with some prior estimates (Ehlig, 1975b; McCulloh and others, 2001). Post-Miocene right slip thus transferred onto the Vasquez Creek Fault southeast of the bifurcation. The right separation on the Vasquez Creek Fault adds to the generally accepted 22-23 km of middle-late Miocene right separation established for the San Gabriel Fault east of the bifurcation (Ehlig, 1981), resulting in total right separation of 34-35 km northwest of the bifurcation.

Clast sizes and lithologies in Saugus Formation deformed alluvial fan deposits in the Gold and Little Tujunga Canyons area indicate that alluvial stream flow was from the north or north-northeast. The alluvial fan complex is beheaded at the San Gabriel Fault Zone, and no correlative deposits have been found north of the fault zone. Likely sources of several distinctive clast types are east of the bifurcation and north of the Vasquez Creek Fault. Combining these data with right slip caused by the 34°±6° of clockwise local block rotation (Levi and Yeats, 2003) suggests that post-Saugus Formation (<2.6 to 0.78 Ma) right separation along the fault zone is 4±2 km.

The fossils, lithology, and age of the Gold Canyon beds correlate with the basal Pico Formation (Oakeshott, 1958). The beds presumably connected southward or southwestward to a more open marine setting. A search for correlative strata to the south and southwest found that some strata previously mapped as Towsley Formation correlate with the Modelo Formation. Oyster spat in some Modelo Formation beds are the first recorded fossil occurrences and are especially remarkable because of associations with Miocene bathyal benthic foraminifers, planktonic calcareous nannofossils, and diatoms. Topanga Group basalt resting on basement rocks between Little and Big Tujunga Canyons gives an age of 16.14±0.05 Ma from $^{40}Ar/^{39}Ar$ analysis. Improved understanding of the upper Miocene stratigraphy indicates large early movement on the eastern Santa Susana Fault at about 7-6 Ma.

Introduction

The San Gabriel Fault Zone, a major zone of right slip in southern California, extends for >128 km from the northwestern corner of the Ridge Basin southeastward to the eastern end of the San Gabriel Mountains (Ehlig, 1975b; Morton, 1975; Dibblee, 1982; Powell, 1993, p. 33-34; Nourse, 2002; Crowell,

[1] U.S. Geological Survey, 345 Middlefield Road, Menlo Park, CA 94025

[2] 7136 Aberdeen Ave., Dallas, TX 75230

[3] Department of Geosciences, University of Texas at Dallas, P. O. Box 830688, Richardson, Texas 75083

[4] Morin Biostratigraphic Studies, 2016 Wedgewood Lane, Carrollton, TX 75006

[5] 11137 Nile River Ct., Rancho Cordova, CA 95670

2003, p. 172; Yeats and Stitt, 2003) (fig. 1). The fault zone branches to the southeast in the western San Gabriel Mountains. The north branch, the San Gabriel Fault, with 22-23 km of right separation (Ehlig, 1968, 1981; Powell, 1993, p. 34; Nourse, 2002), curves eastward from the bifurcation. The south branch, the Vasquez Creek Fault, curves southeastward through the mountains as a right-reverse-slip fault; it merges with the north-dipping reverse Sierra Madre Fault Zone along the southern mountain edge (Dibblee, 1968; Powell and others, 1983; Smith, 1986; Crook and others, 1987) (fig. 1). Slip histories of the San Gabriel and Vasquez Creek Faults are part of the structural evolution of the northern Los Angeles basin region (see, for example, McCulloh and others, 2001; Yeats, 2004).

The Gold Canyon beds are a sequence of partly macrofossiliferous marine sandstone with breccia-conglomerate lenses, exposed over a small isolated area 5.5 km along the San Gabriel Fault Zone northwest of its bifurcation. The beds crop out only in Gold Canyon, a minor southeast-draining tributary to lower Big Tujunga Canyon (fig. 2*A*). These strata, whose approximate age has previously been estimated as late Miocene or Pliocene (for example, Hill, 1930; Oakeshott, 1958), lie on the south fault block and are cut by the fault zone (Hill, 1930; Oakeshott, 1958; Weber, 1982; this report).

Ehlig (1975b, p. 14) recognized clasts from the marginal zone of the Mount Lowe intrusive suite (Morton and Miller, 2003) in the Gold Canyon beds and noted their "closest possible source area…on the north side of the southern branch of the [San Gabriel] fault"; he concluded "a right slip of 7 miles [11 km] would be a minimum displacement along the southern branch of the fault." Our discovery of angular, boulder-size Mount Lowe clasts in multiple polymictic breccia-conglomerate lenses reinforces Ehlig's clast evidence. Ehlig (1975b, p. 14) also states that "lower Pleistocene alluvial sediments of the Saugus Formation are faulted and intensely deformed where they occur along the south side of the San Gabriel Fault Zone in Little Tujunga Canyon, but there is little evidence for major

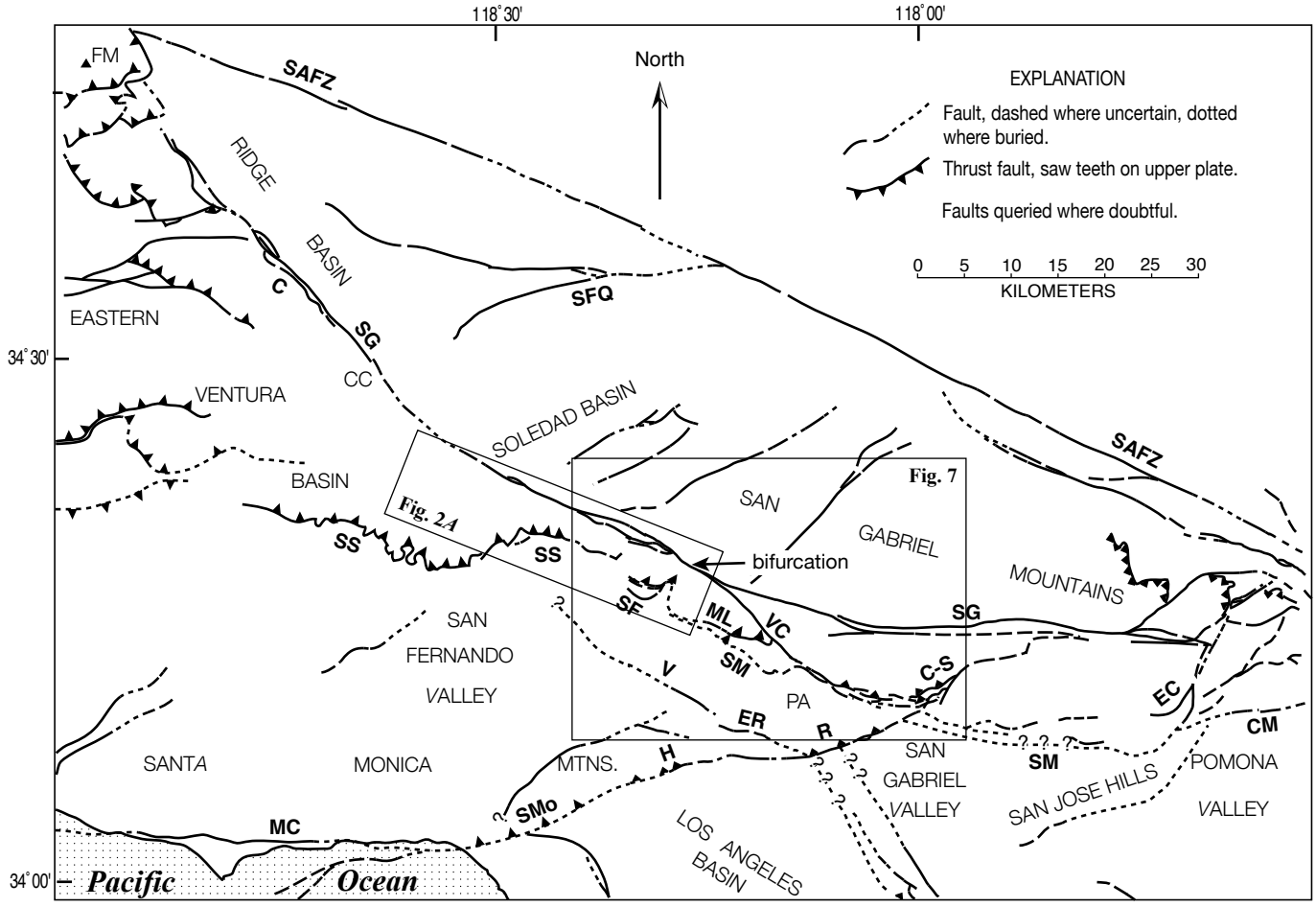

Figure 1. Principal geographic features and simplified fault map of San Gabriel Mountains and surrounding parts of southern California. The San Gabriel Fault bifurcation and areas of figures 2A and 7 are also shown. Fault labels: C, Canton, CM, Cucamonga, C-S, Clamshell-Sawpit, EC, Evey Canyon, ER, Eagle Rock, MC, Malibu Coast, ML, Mount Lukens, R, Raymond, SAFZ, San Andreas Fault Zone, SF, San Fernando, SFQ, San Francisquito, SG, San Gabriel, SM, Sierra Madre-Duarte, SMo, Santa Monica, H, Hollywood, SS, Santa Susana, VC, Vasquez Creek, V, Verdugo. Geographic labels: FM, Frazier Mountain area, CC, Castaic, PA, Pasadena.

strike-slip faulting." However, smaller and better rounded Mount Lowe clasts of the same kind that Ehlig recognized in the Gold Canyon beds also occur in unconformably overlying Saugus Formation fanglomerate in Gold and Little Tujunga Canyons. We reemploy Ehlig's reasoning with other data to postulate some right separation on the San Gabriel-Vasquez Creek Fault Zone since Saugus Formation deposition.

Geologic Setting

Paleocene to Holocene sedimentary units are exposed near the Gold Canyon beds and to the southwest (fig. 2*A*). These units occur above the seismogenic north-dipping eastern Santa Susana and San Fernando reverse fault zones (Wentworth and Yerkes, 1971, p. 13; U. S. Geological Survey, 1971, p. 57; Yeats, 1987, p. 155 and fig. 9-1) or western range-front breaks of the Sierra Madre Fault Zone (Oakeshott, 1958, p. 92; Crook and others, 1987, p. 42). Coarse clastic Neogene units (Oakeshott, 1958, p. 69-85) were derived from San Gabriel Mountains basement rock suites (Jennings, 1977; Ehlig, 1975a; Powell, 1993, appendix 1; Morton and Miller, 2003, p. 146-147; Yerkes and Campbell, 2005, p. 30-33). Neogene strata range from boulder conglomerate to siltstone, with subordinate foraminiferal and diatomaceous beds. These strata present a ~16-m.y. record of complex uplifts of the mountains and alternations of marine and nonmarine clastic deposition. Sedimentation began in shelf to lower slope marine settings close to a rocky shoreline and concludes on Holocene alluvial fans.

The San Gabriel Fault Zone north of the Gold Canyon beds consists of three major strands, the Dillon, De Mille, and Watt Faults (Hill, 1930, p. 146-148; Oakeshott, 1958; Weber, 1982, plates 1*A* and 1*B*; Lee and Schwarcz, 1996). The folded Watt Fault, the oldest strand, cuts the Saugus Formation and Gold Canyon beds (fig. 2*A*). The De Mille Fault cuts the Watt and Dillon Faults and trends to the east-southeast past the bifurcation as the Vasquez Creek Fault (Weber, 1982; Dibblee, 1991b, 2002a). North-south shortening after Saugus Formation deposition is evidenced by the northwest-trending Merrick Syncline and by the Buck Canyon, Lopez, and Sunland reverse faults—breaks that dip north- to northwest and separate basement from overridden sedimentary units (Hill, 1930; Oakeshott, 1958; Kahle, 1975; Ehlig, 1975b) (fig. 2*A*).

Pre-Neogene Rocks

The San Gabriel Mountains expose basement rocks ranging from Paleoproterozoic gneisses to Cretaceous granodiorites (Jennings, 1977; Ehlig, 1975a; Powell, 1993, appendix 1). Three of these basement rock suites, relevant here, are described in appendix 1.

Paleocene Martinez Formation (of Oakeshott, 1958) marine sandstone with thin siltstone interbeds and well-cemented cobble conglomerate containing well-rounded durable clasts are the oldest strata exposed near the Gold Canyon beds. These strata crop out within the San Gabriel Fault Zone in a 12-km-long series of slices extending northwestward from Gold Canyon (Oakeshott, 1958, p. 57-58; Dibblee, 1991a, 1991b) (fig. 2*A*). If these strata once extended east of their present eastern limit, evidence for such an extension is lacking.

Neogene Stratigraphy and Chronostratigraphic Findings

No sedimentary or volcanic strata older than 16 Ma are present in the southwestern San Gabriel Mountains south of the San Gabriel Fault Zone and east of the west-dipping normal Whitney Fault (Oakeshott, 1958, p. 44 and plate 1; Huftile and Yeats, 1996, fig. 5, cross section D; Yeats and Stitt, 2003, fig. 3) (fig. 2*A*). Neogene formations show abrupt large changes in thickness and gross lithology. Few are fossiliferous, and microfossils, where present, are generally the most age-diagnostic forms. Fossil localities referred to here and in the appendixes appear in figures 2*A* and 2*B*. Measurements of $^{87}Sr/^{86}Sr$ were made on macrofossil shell, oyster spat, and fish debris and phosphatic material from a coprolite collected from units possibly correlative with the Gold Canyon beds or other relevant units (appendix 2). Calcareous nannofossils, benthic foraminifers, and diatoms were identified and support most isotopic determinations (appendixes 3, 4, and 5). Abrupt regional thickness changes are portrayed in figure 3. Figure 4 emphasizes time to focus on recognized hiatuses in the depositional record. Numeric ages assigned to key stratal units in these figures are detailed in tables 3-7.

Volcanic Rocks of the Topanga Group

Basaltic andesite flow breccia and basalt flows of middle Miocene age, at least 90 m thick, rest unconformably on basement about 4 km southwest of the Gold Canyon beds (Hill, 1930; Oakeshott, 1958; Barrows and others, 1974; Dibblee, 1991b). The age of agglomeratic basaltic andesite (locality D, fig. 2*B*), probably autobrecciated during flow, is 16.14±0.05 Ma by $^{40}Ar/^{39}Ar$ analysis (appendix 6), augmenting data from presumably correlative 14.5±1 Ma basalt 25 km to the west (Turner, 1970; Weigand and Savage, 1993, p, 97, 99). Originally assigned to the middle Miocene Topanga Formation (of Shelton, 1955, and Oakeshott, 1958), these rocks correlate with part of the Conejo Volcanics Formation of the Topanga Group (Yerkes and Campbell, 1979).

Modelo Formation

Strata correlative with the Modelo Formation are exposed eastward from Pacoima Wash along the south flank of the

Figure 2. Geology of the southwestern San Gabriel Mountains and adjacent area to the west, California. Geology north of the San Gabriel Fault Zone and south of the Sierra Madre, San Fernando, and Santa Susana fault zones is not shown. Shown in *A* or *B* are fossil localities C, and E through X (appendixes 2 through 5), $^{40}Ar/^{39}Ar$-dated basalt locality D (appendix 6), columnar sections C1 through C9 (fig. 3), drill hole localities S and V (fig. 3), and paleomagnetic traverses of Levi and Yeats (1993, 2003). Fault labels: BC, Buck Canyon, D, Dillon, DM, De Mille, L, Lopez, S, Sunland, SF, San Fernando, SG, San Gabriel, SM, Sierra Madre, SS, Santa Susanna, VC, Vasquez Creek, W, Watt, WH, Whitney. Geographic labels: BTC, Big Tujunga Canyon, LTC, Little Tujunga Canyon,

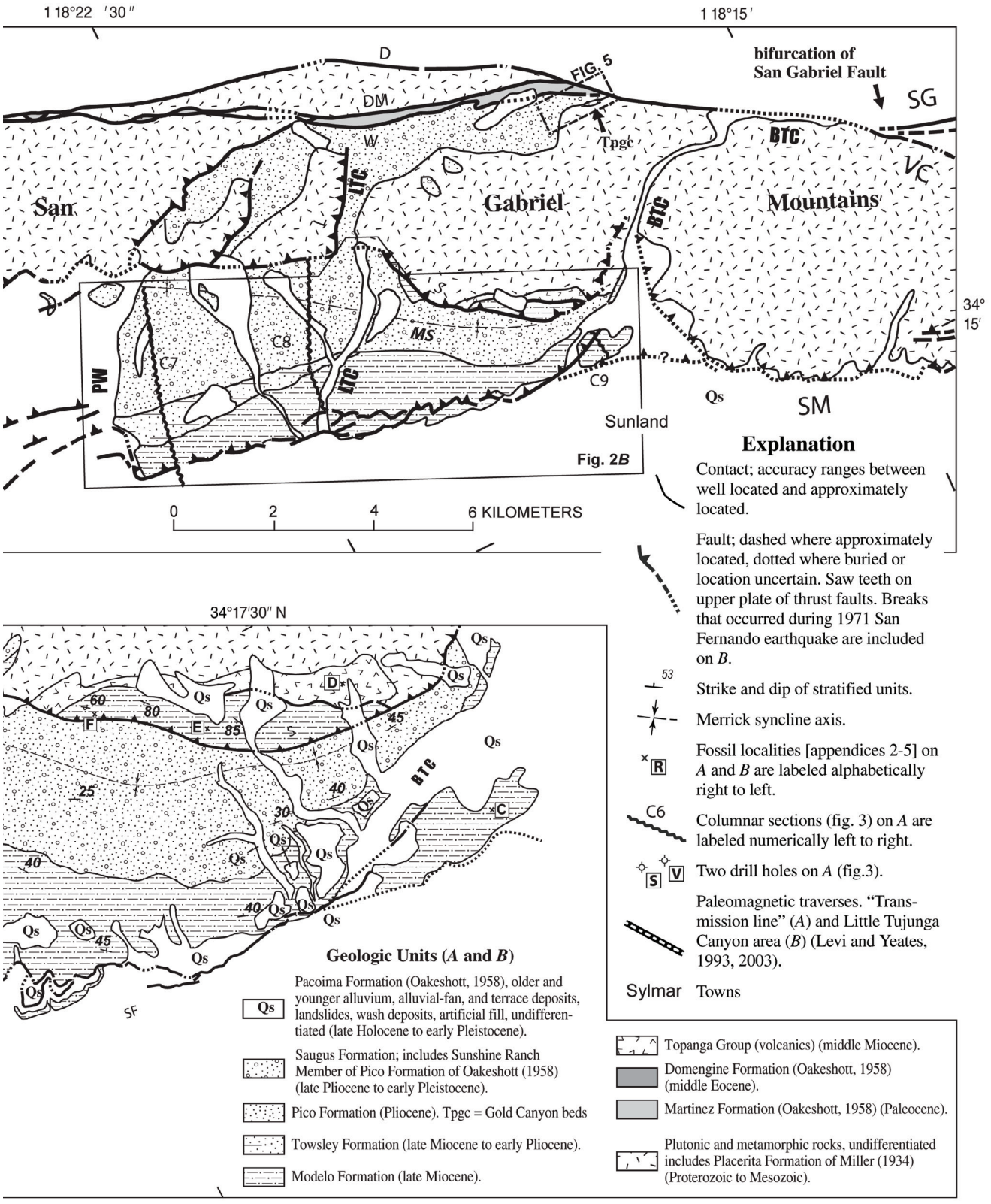

PW, Pacoima Wash, SFP, San Fernando Pass. *A*, Generalized geologic map of the southwestern margin of the San Gabriel Mountains and eastern Santa Susana Mountains adapted from Hill (1930), Winterer and Durham (1962), Barrows and others (1974), Weber (1982), Crook and others (1987), and Dibblee (1991a, 1991b). Inset frames show areas of figures 2*B* and 3. *B*, Geologic map of area between Pacoima Wash and Big Tujunga Canyon with revised Modelo Formation-Towsley Formation contact (adapted and partly simplified from Hill, 1930; Oakeshott, 1958; Barrows and others, 1974; Crook and others, 1987; and Dibblee, 1991a, 1991b). Geology along and near the Sunland Fault is from Dibblee (1991b), based on our mapping and field checks.

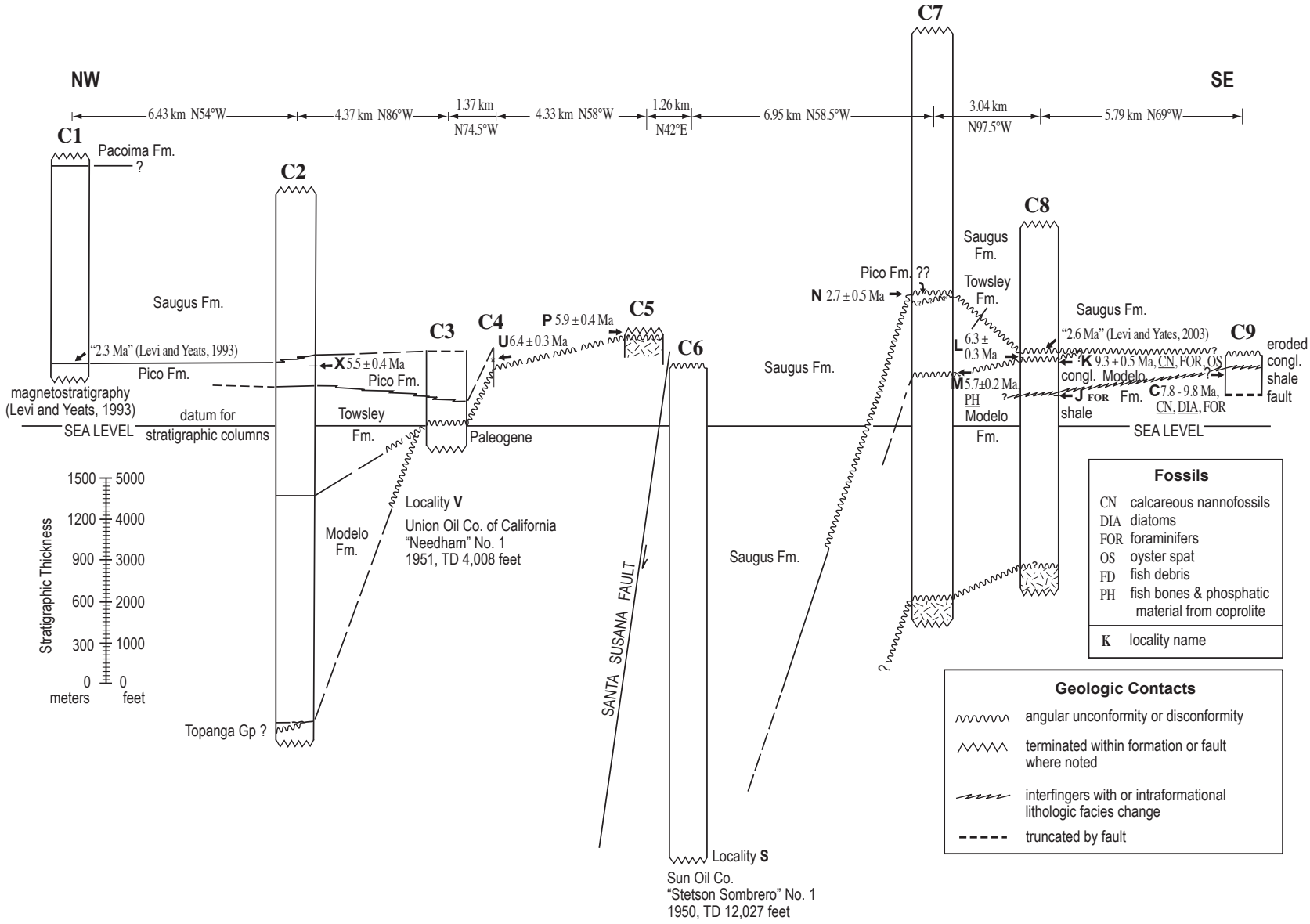

Figure 3. Columnar sections of middle Miocene through middle Pleistocene strata showing inferred correlations from west of San Fernando Pass to mouth of Big Tujunga Canyon. Locations are shown in figure 2*A*. Thicknesses are measured from geologic maps of Oakeshott (1958), Winterer and Durham (1962), Dibblee (1991a, 1991b, 1992), Levi and Yeats (1993), and Wright (2001), tempered by our work. Most age determinations and ranges are based on $^{87}Sr/^{86}Sr$ isotope analyses of marine macrofossil shell material (appendix 2). Underlined exceptions are fish debris (locality M), calcareous nannofossils (locality K), and calcareous nannofossils plus diatoms (locality C) (fig. 2*B*). Ages are labeled with letters that correspond to fossil localities shown in figures 2 and 6, and discussed in the text and appendixes.

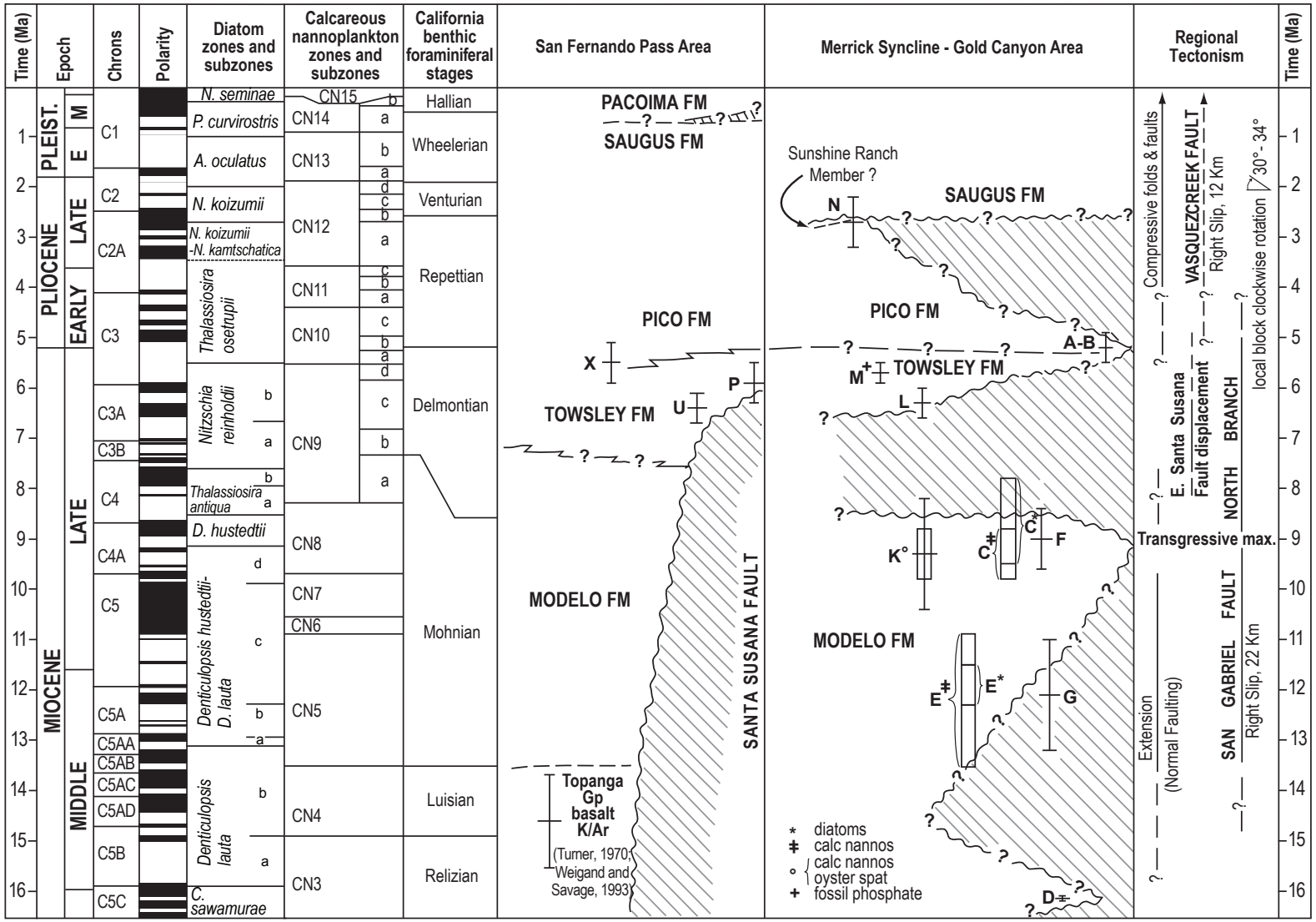

Figure 4. Chronostratigraphic correlation diagram of middle Miocene through middle Pleistocene formations of the Merrick Syncline-Gold Canyon and San Fernando Pass areas. Diagonal striping indicates missing section. Wavy lines denote unconformities or discontinuities. Vertical lines with terminating brackets are $^{87}Sr/^{86}Sr$ age ranges of marine macrofossil shells, fish debris or oyster spat and one $^{40}Ar/^{39}Ar$ basalt age. Vertical rectangles are age ranges of calcareous nannoplankton, and diatoms. Letters correspond to fossil localities discussed in text or shown in figures 2 and 5, and the appendixes. Reference to Sunshine Ranch Member of Winterer and Durham (1958) at site N is hypothetical, to include the possibility that those marine fossils might represent the basal marine member of the Saugus Formation (see also Oakeshott, 1958, p. 82-83). Regional tectonic events reflect our work and the published record. Sources of reference columns are Lourens and others (2004), Barron and Gladenkov, (1995), Barron and Isaacs (2001, fig. 22.1), and Okada and Bukry (1980), with minor adjustments to the benthic foraminiferal stage boundaries. Normal polarity in the magnetic polarity column is shown in black, reversed polarity in white.

Merrick Syncline and also locally on its northeast flank, where they rest unconformably on Topanga Group lavas (Oakeshott, 1958; Dibblee, 1991a, 1991b) (fig. 2*B*). The type Modelo Formation is located in the Santa Monica Mountains about 30 km southwest of Big Tujunga Canyon (Hoots, 1931, p. 102-115; Winterer and Durham, 1962, p. 286-287; Blake, 1991, fig. 5). It ranges in age from the Luisian through part of the Delmontian benthic foraminiferal stages (BFS) (15-14 Ma to 7.7-6.5 Ma, Barron and Isaacs, 2001, p. 394). In the study area, porcelaneous, diatomaceous, and calcareous siltstone and shale occur with subordinate interbedded arkosic sandstone; pebbly sandstone and cobble to boulder conglomerate dominate locally (Oakeshott, 1975, p. 24; Kahle, 1975, p. 120).

We revise the top of the Modelo Formation along the south flank of the Merrick Syncline to be within the Towsley Formation of others (Barrows and others, 1974; Dibblee, 1991a, 1991b). Somewhat lenticular, massively bedded cobble to boulder conglomerate units, previously assigned to the lower part of the Towsley Formation (for example, "Ttog" of Dibblee, 1991a, 1991b), are submarine-canyon or proximal submarine-fan deposits, based on benthic foraminifers from thin, fine-grained, calcareous siltstone interbeds and lenses (localities K and J, fig. 2*B*, and appendix 4). They are faunally equivalent to older parts of the type Modelo Formation. Strata we correlate with the Towsley Formation occur unconformably above these conglomerate beds and consist of more friable, massive to thinly laminated and bioturbated siltstone, with interbedded sandstone and weakly cemented conglomerate. The sandy siltstone beds and lenses, and thin to thick beds of sandy conglomerate (Oakeshott, 1958, p. 76), are consistent faunally and lithologically with marine deposition in outer to inner shelf environments. Near Pacoima Wash our revised Modelo Formation strata are up to 2,000 m thick, but they thin over a short distance to the east (Wright, 2001, fig. 5).

Towsley Formation

The type Towsley Formation (Winterer and Durham, 1958, 1962) contains microfossils of the Delmontian BFS (7.7-6.5 Ma to 5.2 Ma, Barron and Isaacs, 2001, p. 394). Basin-margin marine strata assigned to the Towsley Formation buttress against or onlap the basement complex. These strata occur partly as isolated erosional remnants atop the upper plate of the Santa Susana Fault Zone in the foothills of the westernmost San Gabriel Mountains southeast of San Fernando Pass (Winterer and Durham, 1962, p. 291-292 and fig. 52; Dibblee, 1991a) (fig. 2*A*). South of the Santa Susana Fault Zone and farther east between Pacoima Wash and Big Tujunga Canyon, an eastward thinning sequence of partly shallow-marine sandstone and conglomerate with sandy siltstone and silty claystone is late Miocene to earliest Pliocene in age. Mapped as "Repetto formation" (Oakeshott, 1958, p. 75-78), "Towsley and/or Pico Formations undifferentiated" (Barrows and others, 1974, plate 2), and "Towsley (?) Formation" (Dibblee, 1991a, 1991b), parts of this sequence as described above are reinterpreted here as older Modelo Formation (fig. 2*B*). The thickness of the revised Towsley Formation in Lopez Canyon is 650 m (reinterpreted from Oakeshott, 1958, plate 3, sec. BB', and Dibblee, 1991a).

Pico Formation

Marine siltstone, sandstone, and conglomerate of the Pico Formation ("Fernando Formation" of Yeats and others, 1994, p. 1055) are early to earliest late Pliocene age. These strata interfinger along a diachronous contact with underlying siltstone and fine-grained sandstone of the Towsley Formation west of San Fernando Pass (Winterer and Durham, 1962, p. 308; Squires and others, 2006) (fig. 2*A*). Correlative strata have been mapped just southeast of San Fernando Pass within the Santa Susana Fault Zone (Winterer and Durham, 1962, p. 311 and plate 44) and reported to the south in the northern San Fernando Valley subsurface (Oakeshott, 1958; Tsutsumi and Yeats, 1999). They have not previously been recognized in outcrops between Pacoima Wash and Big Tujunga Canyon. We assign the isolated Gold Canyon beds to the Pico Formation (see below).

Saugus Formation

Alluvial and fluvial strata of the Saugus Formation (Kew, 1924; Winterer and Durham, 1962, p. 317-320; Oakeshott, 1958, p. 83-85; fig. 2*B*) are light gray to buff, moderately consolidated, poorly sorted, coarse- to medium-grained arkosic sandstone interbedded with polymictic pebble to boulder conglomeratic sandstone and conglomerate. Individual beds are lenticular. Conspicuous and locally thick beds of reddish sandy to clayey siltstone to fine-grained sandstone are abundant in the lower part of the section in the Little Tujunga Canyon area (Oakeshott, 1958, p. 84; this study) and may be paleosol or overbank deposits. Conglomerate is coarser grained and more abundant east than west of Little Tujunga Canyon (Oakeshott, 1958, p. 84). Approximately 3,700 m of Saugus Formation fanglomerate was penetrated by a drill hole west of Pacoima Wash (Oakeshott, 1958; Tsutsumi and Yeats, 1999, fig. 4, section FF'; Wright, 2001, fig. 2) (locality W, fig. 2*A*). The fanglomerate sequence thins southeasterly to 2,000 m at Lopez Canyon, 1,300 m just west of Little Tujunga Canyon (Levi and Yeats, 2003, p. 15-5), 600 m 3 km east of Little Tujunga Canyon, and is absent east of Big Tujunga Canyon (Oakeshott, 1958, p. 83-84; Crook and others, 1987) (fig. 2*B*).

The late Pliocene to middle Pleistocene age of the Saugus Formation is based on fragmentary terrestrial vertebrate fossils (Winterer and Durham, 1962, p. 322; Saul, 1975, p. 55). A local age estimate of the Merrick Syncline section is based on analyses of magnetic polarity traverses made about 13 km west ("Van Norman Lake domain") and about 23 km west-northwest ("Transmission Line" or "Magic Mountain domain") (Levi and Yeats, 1993, 2003) (fig. 2*A*). Polarity reversal patterns and correlations, a dated ash, and inferred

sedimentation rates date deposition of both sequences to between 2.3 and 0.5 Ma. Saugus Formation magnetic polarity stratigraphy in Little Tujunga Canyon "suggests deposition during the Matuyama chron, 0.78-2.60 Ma" (Levi and Yeats, 2003) (fig. 2*B*), but the data do not record the Matuyama chron bounding magnetic reversals. We consider the chron to represent bounding time limits only.

Chronostratigraphy: Ancillary Paleogeographic and Structural Implications

A significant hiatus with local evidence of erosion separates 16.14±0.05 Ma Topanga Group volcanic rocks from overlying littoral marine strata of the basal Modelo Formation on the northeast flank of the Merrick Syncline east of Little Tujunga Canyon (localities D, G, and E, fig. 2*B*). Partly pebbly mollusk-bearing Modelo Formation sandstone and siltstone grade upward into foraminiferal and locally diatomaceous, thinly bedded calcareous clayey siltstone and shale. The siltstone and shale are probably older than 11.5 Ma near their base (appendix 5). The original full easterly extent of the basal Modelo Formation beds is unclear, but surface mapping (Oakeshott, 1958; Dibblee, 1991a, 1991b) and an isopach map (Wright, 2001, fig. 5) suggest that the eastern limit of a west-opening mid-Miocene marine embayment may have been at long 118˚17.5'W, about 6 km west-southwest of the San Gabriel Fault bifurcation.

The disconformable base of the Towsley Formation along the south flank of the Merrick Syncline correlates with an unconformity separating fossiliferous basal Towsley Formation strata from basement rocks north of the Santa Susana Fault Zone in the area 4 km northwest of Pacoima Wash. Stratigraphically, localities L and M correlate roughly with locality P near the base of the Towsley Formation (fig. 2*A* and 2*B*, and appendix 2, table 3). The onset of large reverse slip on the Santa Susana Fault Zone of this area (Yeats, 1979, 2001) is thus dated at 7-6 Ma (during the Delmontian BFS). Probably more than 2 km of Modelo Formation strata were eroded from the upthrown north block of the Santa Susana Fault Zone before deposition of the basal Towsley Formation beds at 6 Ma. The base of the Modelo Formation south of the Santa Susana Fault Zone, west of Pacoima Wash, is estimated to be about 6 km below sea level (Wright, 2001, fig. 5). Santa Susana Fault growth was continuing at 5.2 Ma when littoral marine Gold Canyon beds were deposited, suggesting that uplift of the structurally high north block was episodic and subsidence of the south block dominated. Fault growth continued through the Pleistocene, as indicated by the present 700-m elevation of the Gold Canyon beds and by the 3.7 km

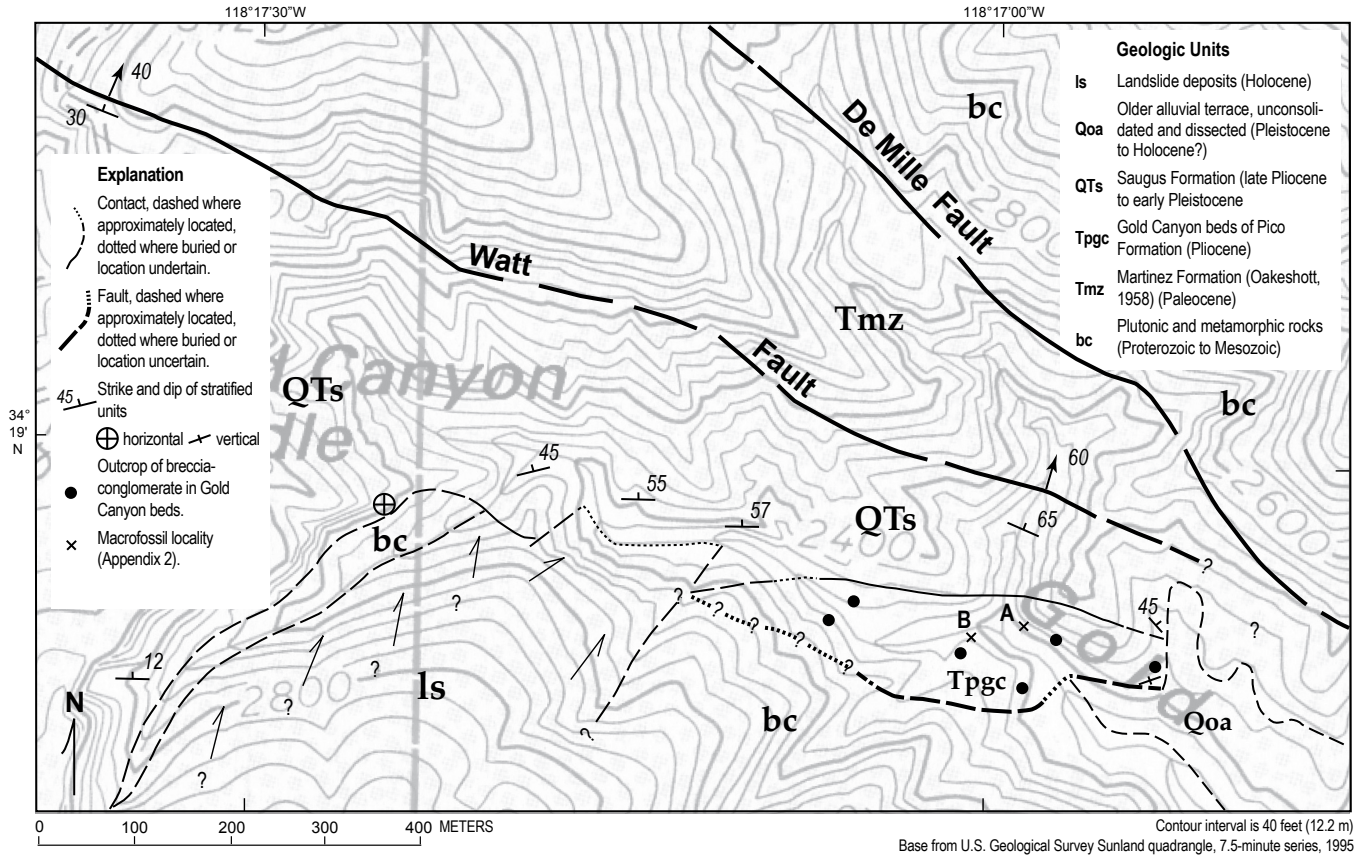

Figure 5. Local geologic map of Gold Canyon beds incorporating our observations (modified from Hill, 1930; Oakeshott, 1958; and Weber, 1982). Macrofossil localities A and B (appendix 2) and observed exposures of breccia-conglomerate in the Gold Canyon beds are also shown.

of Saugus Formation beds penetrated by the Sunray "Stetson-Sombrero" No. 1 drill hole (Oakeshott, 1958, p. 122; locality S, fig. 2*A*). The 1971 M_W 6.7 Sylmar earthquake, whose epicenter is 6 km north of the southwest end of the Buck Canyon Fault (fig. 2*A*), indicates that both the south and north blocks continue to rise differentially (Allen and others, 1975; Savage and others, 1975; Tsutsumi and Yeats, 1999).

Gold Canyon Beds

The Gold Canyon beds are exposed in an isolated area, 100 m by 400 m, south of the Watt Fault in upper Gold Canyon. They are the easternmost known exposures of fossiliferous marine strata adjacent to the San Gabriel and Vasquez Creek Faults within the San Gabriel Mountains (fig. 5). They are mostly north dipping; some very poorly stratified breccia-conglomerate lenses may be south dipping, but such attitudes are questionable. The base of the sequence is unexposed, but might be an unconformity or fault that dips steeply north and strikes roughly N. 70° W. The sequence is overlapped to the west by the base of the Saugus Formation. The junction of the Watt Fault and the younger De Mille Fault to the northeast is obscured by colluvium and older alluvium. These faults cut off the easternmost Gold Canyon beds and Saugus Formation fanglomerate units (fig. 5).

The estimated thickness of exposed Gold Canyon beds is less than 100 m. The dominant rock type is massive, light gray to light gray-brown medium- to fine-grained arkose, partly fractured and oyster bearing (fig. 6*A*). Parts are pebbly or conglomeratic, with polished well-rounded granitoid and gneissic cobbles. Some gneiss cobbles contain rutilated quartz, suggestive of Paleoproterozoic Mendenhall Gneiss (Oakeshott, 1958; appendix 1). Subordinate rock types are (1) fractured, dark gray-brown arkose containing rutilated quartz grains, (2) poorly sorted polymictic cobble to boulder breccia-conglomerate lenses with green-brown (partly reddish) arkose to arkosic grus matrices containing rutilated quartz grains (fig. 6*B*), and (3) thin-bedded, dark gray biotitic arkose.

Multiple horizons of lenticular breccia-conglomerate contain angular to rounded clasts derived from the Mount Lowe intrusive suite. Some angular to subangular Mount Lowe clasts as large as 1 m are matrix supported. Smaller clasts are subrounded to rounded (fig. 6*B*). Subangular to subrounded gneissose clasts in these lenses have granoblastic textures and rutilated quartz (appendix 1). Dark colored and nondurable subangular clasts as large as boulder size are biotite epidote hornblende arkose (one containing an altered foraminifer shell), derived from the distinctive but fault-separated Paleocene Martinez Formation (Oakeshott, 1958) marine strata (fig. 5). No clasts from the "anorthosite-syenite complex" (Powell, 1993, p. 81; also appendix 1) were found. Sources of the large and mostly angular clasts include the Mount Lowe intrusive suite, exposed today north of the Vasquez Creek Fault 12 km to the southeast, and the Paleocene Martinez Formation (Oakeshott, 1958) exposed today only to the north and northwest between strands of the San Gabriel Fault Zone (figs. 2*A*, 5).

Although macrofossils are abundant in parts of the Gold Canyon beds, age-diagnostic fossils are lacking. More than 90 percent of fossil oyster shells examined in the uppermost (and relatively fossiliferous) part are ≥12.5 cm long and thick shelled, with pearly-lustered laminae. However, most intact shells are pervasively fractured. Many separate clusters of multiple shells occur. These oysters may be *Crassostrea* sp. (C.L. Powell, II, oral commun., 2004). Less common are separate aggregations of shell fragments with rare indeterminate gastropod and pectinid fragments. One 6-cm-long poorly preserved gastropod, possibly *Kelletia* sp., an echinoid fragment, bits of two different crab dactyles (moveable fingers) (C. L Powell, II, oral commun., 2004), and one 4-cm shell fragment of *Lyropecten* (?) sp. (J. G. Vedder, oral commun., 2008) were found. The nondiverse oyster-dominated fauna suggests a shallow, nearshore marine environment, possibly with restricted circulation and brackish water. The absence of shells in growth positions and the loose aggregates of smaller broken shell fragments indicate some transport before deposition (fig. 6*A*). No microfossils were found.

Our age for deposition of the Gold Canyon beds is 5.2±0.3 Ma (earliest Pliocene), based on $^{87}Sr/^{86}Sr$ analyses of multiple fossil carbonate samples from five selected oysters and one pecten fragment (appendix 2, table 3) (localities A and B, fig. 5). This age, close to the Miocene-Pliocene boundary (Barron and Isaacs, 2001, p. 394), is correlative with either youngest Towsley Formation or oldest Pico Formation. The shallow-marine depositional environment and fauna suggest correlation with the basal part of the Pico Formation (Winterer and Durham, 1962). Prior age assignments of the Gold Canyon beds range between questionable latest Miocene and early Pliocene (Hill, 1930; Oakeshott, 1958. p. 77; Ehlig, 1975b; Weber, 1982, p. 65; Dibblee, 1991b).

Possible Correlative Strata

Our chronostratigraphic observations south and southwest of the Gold Canyon beds suggest strata possibly correlative with the Gold Canyon beds. The revised Towsley Formation south of the Santa Susana Fault thins eastward from Pacoima Wash to Little Tujunga Canyon by erosional truncation at the base of the overlying Saugus Formation. The base of the Towsley Formation is dated at about 6 Ma (localities L, M, and P, fig. 2*A* and 2*B*, and appendix 2, table 3) and is above a disconformity or correlative unconformity. Where not eroded, the top is a slight erosional angular unconformity with a minimum age of about 3 Ma (locality N, fig. 2*B*, and appendix 2, table 3). The macrofossiliferous shallow-marine sandstone of this youngest part of the Towsley Formation, just east of Pacoima Wash, might correlate with oldest Pico Formation. The upper half of the section assigned to the Towsley Formation just east of Pacoima Wash might include unidentified 5.2 Ma strata correlative with the Gold Canyon beds, judging from fossil ages at localities M and N (fig. 2*B*).

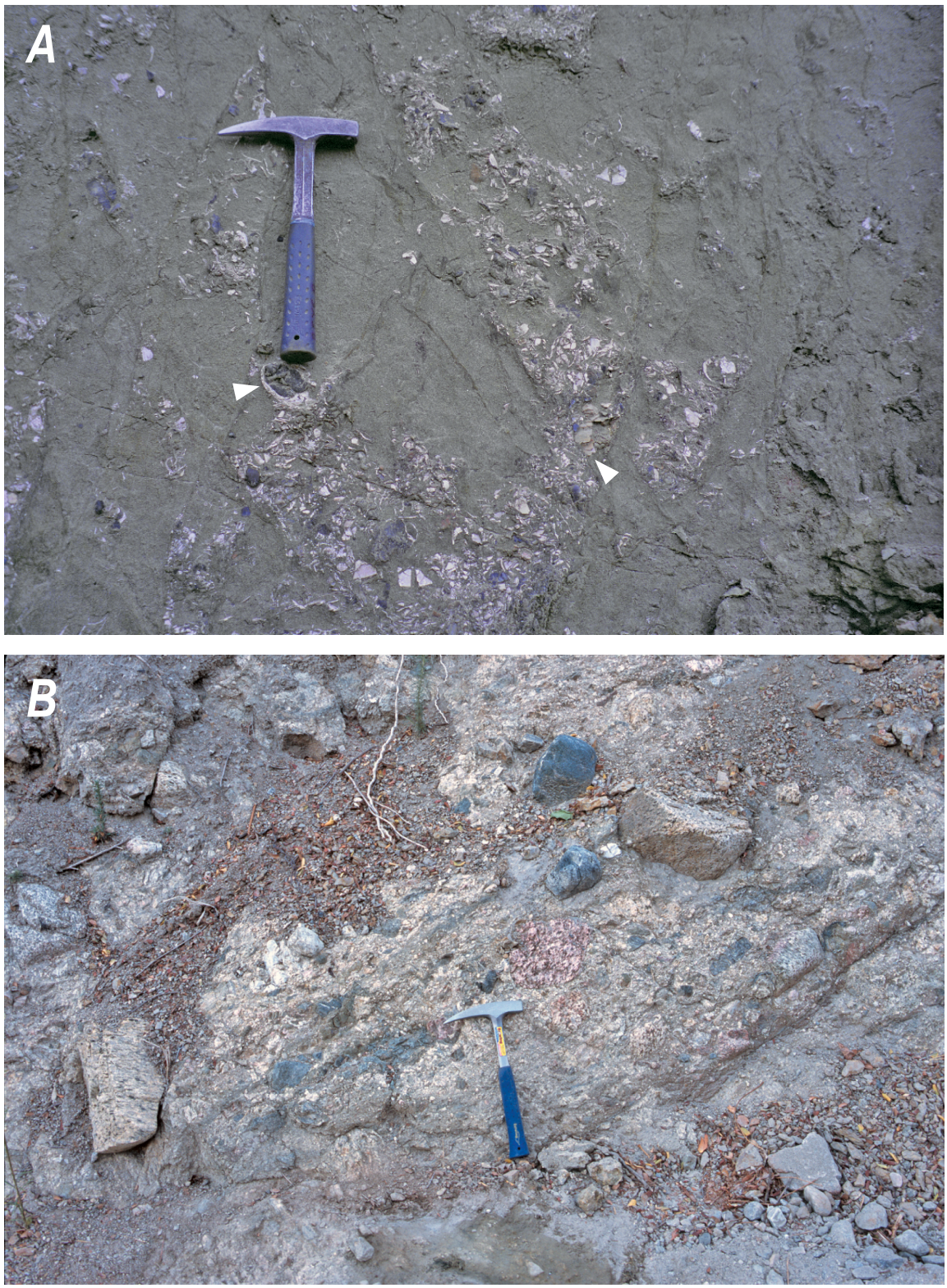

Figure 6. Rock types in the Gold Canyon beds. *A*, Rain-dampened fossiliferous sandstone of the Gold Canyon beds showing some intact but fractured oyster shells (white arrowheads) plus abundant oyster shell fragments and associated very rare gastropods, bivalves, and crab fragments. Hammer is 32 cm long. *B*, Polymictic breccia-conglomerate lens of the Gold Canyon beds containing two prominent angular to subangular boulders (lower left and upper right) from the marginal facies of the Mount Lowe intrusive suite (appendix 1). These boulders, together with multiple smaller angular to subrounded Mount Lowe clasts, dominate the clast population at this outcrop.

Table 1. Estimates of amount and timing of right separation on the Vasquez Creek Fault, together with evidence for offset magnitude, from published sources and this study.

Author (publication date)	Estimate of Vasquez Creek Fault right separation	Estimate of time interval of slip	Evidence of offset	Remarks
Oakeshott (1958, 1975)	unspecified	unspecified	"Right-lateral strike-slip movement on the San Gabriel fault has probably been on the order of 4 miles [~6 km] in Quaternary time, judging by displacement of older faults and sediments that lie on the crystalline rocks" (Oakeshott, 1975, p. 27)	Observations of apparent right offset that range from 1 1/2 to 4 miles [~2 to ~6 km] were observed westward from the bifurcation of the San Gabriel Fault to about long 118°30′W (Oakeshott, 1958, p. 91-92). Displacements on the Vasquez Creek Fault and northwesternmost San Gabriel Fault are not discussed.
Ehlig (1975b)	11 to 32 km	after depostion of "gravel lens" in Pliocene marine sandstone in Gold Canyon	"Gravel lens" within sliver of fossiliferous Pliocene marine sandstone along the south side of the San Gabriel Fault in Gold Canyon (here the Gold Canyon beds) contains pebbles and cobbles of Mt. Lowe intrusive suite. "The closest possible source area is on the north side of the southern branch of the fault [Vasquez Creek Fault], 7 miles [~11 km] to the east" and "furthest possible source area is more than 20 miles [~32 km] to the east" (Ehlig, 1975b, p. 14).	No clasts of anorthosite or Mendenhall Gneiss were observed in the gravel lens (Ehlig, 1975b, p. 14). Ehlig's range of estimated right separation on the Vasquez Creek Fault added to his generally accepted estimate of 22 km of right separation on the San Gabriel Fault east of its bifurcation results in a range of 33 to 54 km of right separation on the San Gabriel Fault west of its bifurcation.
Weber (1982, 1988a)	unspecified	unspecified	No measures are specified of total offset eastward from San Gabriel Fault crossing of upper Pacoima Canyon, but multiple observations of small offsets of streams and older alluvial deposits suggest apparent right, left or reverse motion on various strands of the fault zone (Weber, 1982, p. 38-47).	"At least in late Quaternary time, the segment of the [San Gabriel] fault from Castaic to Pasadena, including the South branch [Vasquez Creek Fault], has consisted of a north-dipping reverse fault with a component of right slip..." (Weber, 1988a, p. IV-68). "Total right-lateral offset of Precambrian gneiss and anorthosite along the San Gabriel fault [nortwestward from the westernmost San Gabriel Mountains] is not more than 30 km, and is more likely about 5 km" (Weber, 1988b, p. 236).
Matti & Morton (1993)	22 km		Right separation of 22 km is hypothesized on the Vasquez Creek Fault (their "south branch" of the San Gabriel Fault) that transfers eastward along the south margin of the San Gabriel Mountains to offset the northeast end of the Raymond Fault about 22 km from a hypothetical connection to the southwest end of the Evey Canyon Fault (Matti and Morton, 1993, p. 125-127, Fig. 6*E*).	Reconstruction accepts 22 km of right separation (Ehlig, 1968) on the San Gabriel Fault east of its bifurcation (their "north branch" of the San Gabriel Fault) following slip on the Vasquez Creek-Sierra Madre faults. Thus the San Gabriel Fault west of its bifurcation displays 22+22=44 km of right separation. Powell and Weldon (1992, p. 457) believe projection of "large dextral displacement [eastward] along the south flank of the San Gabriel Mountains is not supported by paleogeologic patterns and is disallowed by the continuous distribution of the 15 m.y.-old Glendora Volcanics across the projected fault path."
Powell (1993)	5 km	3-4 km from 6 or 5 to 4 Ma; 1-2 km from 4 or 3 Ma to present (Powell, 1993, p. 43-44)	Proposes that 5 km of right separation on the Vasquez Creek Fault is "consistent with the distribution of Cretaceous quartz diorite and monzogranite...and realigns the Mount Lukens and Clamshell-Sawpit faults. Conversely, the distribution of crystalline rock units along the Vasquez Creek fault...seems to preclude large lateral displacement on that fault. Restoration of any displacement greater than a few kilometers results in a misalignment and apparent repetition of the quartz diorite line in the southern San Gabriel Mountains" (Powell, 1993, p. 37; also see Powell and others, 1983).	Review of published work led Powell (1993, p. 36-38) to conclude that there is no "compelling paleogeologic reconstructions" or "unambiguous piercing points" that justify more than the 40 to 45 km of total right separation on the northwesternmost San Gabriel Fault. His 40-45 km of right separation seems primarily based on the apparent right offset by the San Gabriel Fault of the San Franciscquito Fault from the Frazier Mountain-Mount Pinos stretch of the San Andreas Fault. This is required by his reconstructions (Powell, 1993; also see Powell and Weldon, 1992; Weldon and others, 1993, p. 187-188). Powell (1993, p. 40, 43-44, Fig. 14) assigns the earliest 13 km of right separation "to the Canton fault and its hypothetical extension." The next 21-23 km is assigned to the San Gabriel Fault and its stretch east of its bifurcation in the San Gabriel Mountains (after Ehlig, 1968). The youngest 5 km is assigned to the Vasquez Creek Fault.

Table 1.—Continued.

Author (publication date)	Estimate of Vasquez Creek Fault right separation	Estimate of time interval of slip	Evidence of offset	Remarks
McCulloh and others (2001)	12-13 km	≤ 7 Ma (possibly ≤ 4.5 Ma)	Latest middle Miocene palinspastic reconstruction of 12-13 km of right separation on the Vasquez Creek Fault plausibly realigns disrupted western edge of field of unique Oligocene dacitic intrusive bodies (McCulloh and ohthers, 2001, p. 22-23, Figs. 6 and 10). Distributions of unique dacitic clasts in middle Miocene conglomerates south of the mountains are favorably restored to locations that correlate well to dacite clast source areas, as are dismembered Paleogene basin-edge deposits and the middle Miocene strandline (McCulloh and others, 2000; 2001, Fig. 11). Reconstruction reconnects the Mount Lukens Fault with the north break of the Clamshell-Sawpit Fault Zone.	Reconstruction requires that (1) right separation on the Vasquez Creek Fault passed via the Sierra Madre Fault Zone to the north-dipping south break of the Clamshell-Sawpit Fault Zone where at least part of the displacement was converted to dip-slip and (2) 22 km of right separation occurred earlier on the San Gabriel Fault east of its bifurcation. Left separation on the Santa Monica-Hollywood-Raymond Fault Zone of 13-14 km coordinates with clockwise rotation of the block north of these faults and south of the Vasquez Creek Fault (McCulloh and others, 2001, p. 17-23, Figs. 9 and 10).
Nourse (2002)	15 km	12-9 Ma	Proposes 37 km of total right separation on the easternmost part of the San Gabriel Fault. Reconstruction transfers westward right separation of 22 km to the San Gabriel Fault and 15 km to a connected Clamshell-Sawpit-Sierra Madre-Vasquez Creek fault system (Nourse, 2002, p. 180-182, Figs. 6, 7,and 8).	Nourse adds 5 km of late Miocene right separation on the northwest San Gabriel Fault, absorbed by extension or transtension in the Los Angeles Basin, to concur with Powell's (1993) 42 km of total right separation there (15+22+5=42 km). Nourse concurs with the Matti and Morton (1993) hypothesis that displacement on the Clamshell-Sawpit-Sierra Madre-Vasquez Creek fault system preceded (12-9 Ma) movement on the San Gabriel Fault east of its bifurcation (9-5 Ma).
Crowell (2003)	22-23 km	ca. 12 to ca. 5 Ma	Crowell (2003, p. 174) concludes that 45 km of right separation passed into the western San Gabriel Mountains from the northwest portion of the San Gabriel Fault. He accepts 22-23 km of right separation on the San Gabriel Fault east of its bifurcation (Ehlig, 1968) and assigns the remaining 22-23 km of right separation to the Vasquez Creek Fault.	Crowell (2003, p. 157,195-196) assigns 80 km of right separation to the northwesternmost San Gabriel Fault. Following the hypothesis of Powell (1993; also see Stitt and Yeats, 1982), he apportions 35 km (instead of Powell's 13 km) of the earliest separation (from ca. 16-11 Ma) to the Canton Fault.
this paper	4 ± 2 km	≤ 2.6 to ≤ 0.8 Ma	The most proximal facies of the Saugus Formation is near the head of Gold Canyon where the distribution of clast size implies transverse sediment transport across the San Gabriel Fault Zone. The mapped boundary of Saugus Formation with and without Mount Lowe intrusive suite clasts against the San Gabriel Fault Zone west of Gold Canyon defines separately sourced parts of a beheaded alluvial fan complex. These facts together with a hypothetical link between fault right slip and local tectonic block rotation, coupled with mean fault slip rate, imply that post-Saugus Formation right separation on the San Gabriel and Vasquez Creekf faults might be about 4 ± 2 km.	Saugus clast size distribution in upper Gold Canyon and areas to the west and southwest suggests sediment transport toward the west-southwest. Added counterclockwise backrotation of 34° (Levi and Yeats, 2003) indicates original sediment transport direction was more orthogonal than parallel to the San Gabriel Fault Zone. Largest Mount Lowe intrusive suite clasts in Gold Canyon suggest transport distances compatible with their transport from sources in an ancestral upper Big Tujunga Canyon drainage system.

Table 1. Estimates of amount and timing of right separation on the Vasquez Creek Fault, together with evidence for offset magnitude, from published sources and this study—Continued.

Author (publication date)	Estimate of Vasquez Creek Fault right separation	Estimate of time interval of slip	Evidence of offset	Remarks
this paper	12 ± 2 Km	≤ 5.2 0.3 Ma	Multiple outcrops of breccia-conglomeratic lenses in the ca. 5.2 Ma-old Gold Canyon beds contain Mount Lowe intrusive suite clasts, including angular to subangular boulders that indicate short transport distances. Nearest cross-fault source for these large clasts are Mount Lowe intrusive suite outcrops north of the Vasquez Creek Fault in the drainage of Arroyo Seco and adjacent canyons to the east (strengthening the observations and corroborating the conclusions of Ehlig, 1975b, p. 14).	Use of modern drainages for ancestral sediment routes is risky, especially when the effects on drainages of rapid Quaternary uplift along the south mountain front, including some reverse motion on the San Gabriel and Vasquez Creek faults, are unmeasured.

The basal Saugus Formation unconformity along the south limb of the Merrick Syncline cuts out all Towsley Formation strata immediately east of Little Tujunga Canyon. Farther east the eroded top of the Modelo Formation is unconformably beneath Saugus Formation fanglomerate (fig. 2*B*). Towsley Formation strata have not been mapped on the north limb of the Merrick Syncline, but might be hidden there by the Sunland reverse fault (Oakeshott, 1958; Barrows and others, 1974; Dibblee, 1991b) (fig. 2*B*). The erosional unconformity at the base of the Saugus Formation, clearly evident on the south limb of the syncline, probably extends northeastward to the faulted north limb where only older Modelo Formation strata and Topanga Group lavas crop out north of the Sunland Fault. Strata correlative to the Gold Canyon beds are missing there.

Right Separation on the Vasquez Creek Fault

Published estimates of Vasquez Creek Fault right separation range between 5 and 32 km (table 1). Estimates of the time of onset of slip range from 12 to 4.5 Ma. Estimates of the cessation of slip range from 9 Ma to present. Only two published studies use offset features along or near the Vasquez Creek Fault, and these give right separation estimates of 5 km (Powell, 1993) and 12-13 km (McCulloh and others, 2001). The age of the Gold Canyon beds, their clast composition, and clasts in the Saugus Formation clarify post-Miocene right separation on the De Mille-Vasquez Creek Faults. Mount Lowe intrusive suite clasts in both the Gold Canyon beds and Saugus Formation have mapped source outcrops (now displaced to the east) located north of the De Mille-Vasquez Creek Faults (fig. 7). Clasts of anorthosite-leucogabbro and other Proterozoic basement types in Saugus Formation fanglomerate beds, together with their source outcrops (fig. 7), are not definitive but are compatible with our findings.

Probable Source of Mount Lowe Intrusive Suite Clasts in the Gold Canyon Beds: Constraints on Vasquez Creek Fault Displacement

Mount Lowe boulders in the Gold Canyon beds are the main basis for attempts to interpret Vasquez Creek Fault offset and corroborate or modify Ehlig's (1975b, p. 14) suggestion of "minimum displacement" of "7 miles" [11 km] on the "south branch." The angularity and size of the largest Mount Lowe boulders in the Gold Canyon beds (location 1 on fig. 7) make long-distance transport unlikely except by landslide or debris flow. Because the trends of the Vasquez Creek-Sierra Madre Faults and the south boundary of the Mount Lowe intrusive suite are nearly parallel north of Pasadena (fig. 7), multiple hypothetical restoration points are possible. The crossing of the Arroyo Seco by the Vasquez Creek Fault (location 2 on fig. 7), the point at which the fault presently is closest to present-day Mount Lowe outcrops, is taken conservatively as a hypothetical minimum restoration point for the Gold Canyon beds containing Mount Lowe boulders. (Areas east of Arroyo Seco also offer short transport distances for Mount Lowe debris but would require even more right separation on the Vasquez Creek-Sierra Madre Faults.) Fault displacement from location 1 to location 2 (fig. 7) would entail 12±2 km of right separation on the DeMille-Vasquez Creek Faults after 5.2 Ma, absent hypothetical fault-parallel clast transport.

Drainage systems during deposition of the Gold Canyon beds can only be inferred. Fault-parallel sediment transport by debris flows in river channels is hypothetically possible and might require less than Ehlig's (1975b) and our estimates of fault offset. However, no evidence was found for fault-parallel clast transport that would shorten our 12±2 km right separation estimate. The angularity of the larger Mount Lowe boulders and the presence of angular nondurable Martinez Formation (Oakeshott, 1958) arkose clasts are inconsistent with the increased clast travel distance. The largest angular Mount

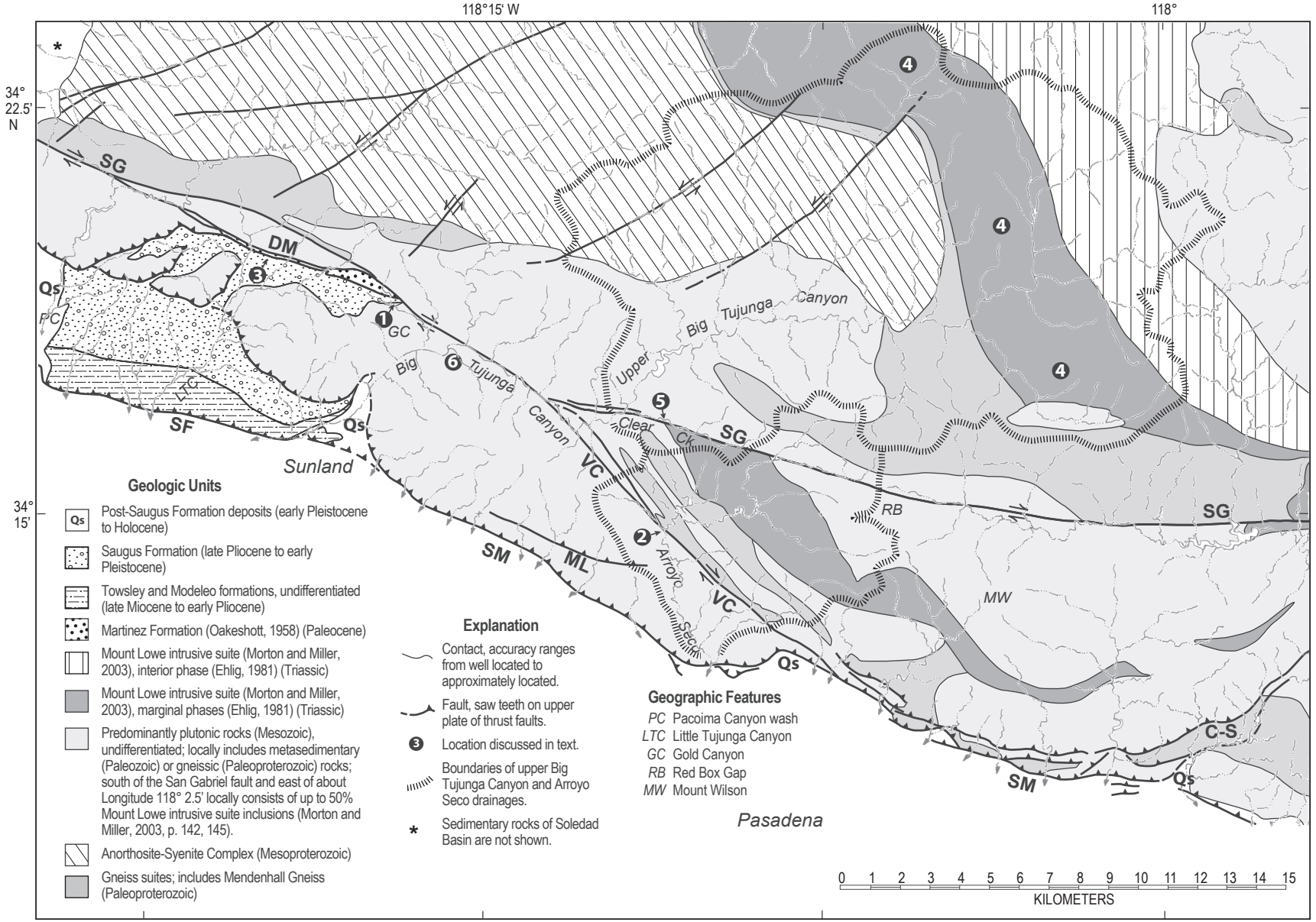

Figure 7. Simplified geologic map of the central and western San Gabriel Mountains emphasizing mapped outcrops of Mount Lowe intrusive suite, anorthosite-syenite complex, and Paleoproterozoic gneiss suite, together with selected faults (adapted from Oakeshott (1958), Carter and Silver (1972), Morton (1973), Ehlig (1981), Weber (1982), Powell and others (1983), Crook and others (1987), Dibblee (1989, 2002a, 2002b), Nourse (2002), and Morton and Miller (2003)). Distinctive Mount Lowe clasts in Gold Canyon beds and Saugus Formation are derived from the marginal phases of the intrusive suite. White-on-black circled numbers are key locations discussed in the text. Upper Big Tujunga Canyon and Arroyo Seco drainage areas, Clear Creek, and selected geographic features are also shown. Fault labels are as in figures 1 and 2.

Lowe clasts, less rounded than comparably sized Mount Lowe boulders in Arroyo Seco gravels at the Vasquez Creek Fault crossing, likely eroded from steep slopes or cliffs. The Martinez Formation clasts imply that Paleocene rocks between the Watt and De Mille Faults were proximal to the Gold Canyon beds during their deposition. They also show that clast transport was from north to south for the larger angular clasts in the breccia-conglomerate lenses of the Gold Canyon beds.

The poorly stratified and ill-sorted breccia-conglomerate lenses with both large angular and smaller rounded clasts are interpreted as landslide or debris flow deposits that entrained some traction-transported clasts in channels during movement from steep terrain to a nearshore marine shelf or estuary. Debris flows from short peripheral drainages along the south margin of the San Gabriel Mountains (for example, Scott, 1971) might be modern analogs.

Clasts of anorthosite and related gabbroic rocks were not found in the Gold Canyon beds (Ehlig, 1975b, p. 14; this study). The anorthosite-syenite complex was shedding debris before, during, and after deposition of the Gold Canyon beds, judging from the scattered occurrences of anorthosite clasts in conglomeratic beds of both the Modelo and Saugus Formations between Pacoima Wash and Big Tujunga Canyon, and in the Towsley Formation west of San Fernando Pass (Oakeshott, 1958, p. 70, 76, 84; Merifield, 1958, 11, 14, 20; Winterer and Durham, 1962, p. 290). The absence of such clasts in the breccia-conglomerate lenses, sequences that represent very short time spans, may be coincidental or because coeval source drainages, while tapping Mount Lowe intrusive suite terrain, did not extend far enough northward to reach the anorthosite-syenite complex. Rutilated quartz in clasts and as matrix grains of the Gold Canyon beds are interpreted as possibly derived from the older Mendenhall Gneiss (Oakeshott, 1958; appendix 1).

Saugus Formation Clasts, Probable Cross-Fault Sources, and Relevant Perspectives

We interpret post-Saugus Formation right separation on the De Mille-Vasquez Creek Faults to be about 4 km. This interpretation is based on (1) a scheme of local tectonic block rotation based on paleomagnetic declinations, (2) mapped distribution of maximum clast sizes, dominant bed-forming process, and Mount Lowe intrusive suite clasts in Saugus Formation beds, (3) fault truncation of a clast lithofacies boundary within the Saugus Formation, and (4) relative abundances of Mount Lowe and anorthosite-syenite complex clasts and types of anorthosite-syenite clasts.

Local Tectonic Block Rotation

The hypothetical role of post-Saugus Formation local block rotation in the Little Tujunga Canyon area is one independent line of evidence. Three paleomagnetic "domains" (structural blocks) with horizontal dimensions on the order of 10-20 km occur in hanging walls of the Santa Susana and San Fernando Fault Zones southwest of, but adjoining, the San Gabriel Fault Zone; two of the three blocks record large clockwise rotations (Levi and Yeats, 2003, p. 15-10 and fig. 9). Regional late Cenozoic dextral shear and associated rotational torques favored clockwise block rotation (Levi and others, 2005, p. 401). "The magnitudes and sense of domain rotations depend on factors including their sizes, shapes, and interactions along boundaries with neighboring domains and adjacent structural elements" (Levi and Yeats, 2003, p. 15-10). The "Merrick Syncline domain" is bounded on the west and east by the Pacoima Wash ("Pacoima segment boundary") and lower Big Tujunga Canyon ("Sunland segment boundary"), respectively, and on the north and south by the San Gabriel and San Fernando or Verdugo Faults, respectively; it has rotated 34˚±6˚ clockwise (Levi and Yeats, 2003, p. 15-8 and fig. 11). Studies showed "no stratigraphic, time-dependent pattern of the Matuyama declinations, indicating that the rotations did not commence until the youngest Matuyama strata [of the Saugus Formation] were deposited" or after 2.6 to 0.78 Ma (Levi and others, 2005, p. 404). Abrupt changes in the trends of folds and of the San Fernando Fault Zone at the Pacoima segment boundary led Levi and Yeats (2003, p. 15-12 and fig. 11) to select a vertical-axis pivot point there. They calculated 6 km of left separation on the Sunland segment boundary in Big Tujunga Canyon. They rejected, as we do, a pivot axis at the Verdugo Fault.

Our hypothesis interprets the 34° of clockwise rotation of the Saugus Formation in the Merrick Syncline block as associated with rotational torque caused by dextral shear on the De Mille Fault. Strike separation along both the San Fernando and Verdugo Faults after 13.6 Ma (end of youngest Topanga Group deposition south of the Verdugo-Eagle Rock Faults) has been shown to be negligible (McCulloh and others, 2001, p. 22 and figs. 5 and 6). Three hypothetical vertical pivot-axis points illustrate the possible right separations on the combined De Mille-Vasquez Creek Faults related to the block rotation. The first two pivot axes (P1 and P2 on fig. 8) are at contrasting locations in the Pacoima segment boundary used by Levi and Yeats (2003). They give 2.1 km and 4.3 km of right separation on the De Mille Fault. The third pivot axis on the south flank of the Merrick Syncline just west of Little Tujunga Canyon, roughly in the center of the block and closest to the paleomagnetic declination measurements, gives 3.4 km of right separation (point P3 on fig. 8). Calculations assume that all dextral shearing between the rotated block and the presumably nonrotated region northeast of the San Gabriel Fault Zone is concentrated along the De Mille Fault and that all torque coupling manifests as block rotation. The measured 34° of clockwise rotation of the Merrick Syncline block is thus consistent hypothetically with as much as several kilometers of right separation on the combined De Mille-Vasquez Creek Faults since 2.6 to 0.78 Ma. Imperfect torque coupling to the rotating block would mean even more right separation.

Clast Size, Bed-Forming Process, and Distribution of Mount Lowe Clasts

Saugus Formation fanglomerate coarsens to the north and east. Locally dominant interbeds of reddish fine- to coarse-grained sandstone occur throughout the area. In the area east of Little Tujunga Canyon, some clasts are as much as 1.2 m in diameter and bedding "becomes almost indistinguishable" (Oakeshott, 1958, p. 84). Clasts exceed 1.7 m in size in upper Gold Canyon, where debris-flow units are coarsest and most abundant (fig. 9). Fanglomerate beds near the head of Gold Canyon are the most proximal facies of the relatively large alluvial fan system bearing Mount Lowe clasts. Figure 10 shows maximum size of Mount Lowe clasts and of all clasts, together with dominant bed-forming process (debris-flow or fluvial-flow). (See also appendix 1, table 2). These inconclusive data hint that sediment transport direction was to the west-southwest or southwest, roughly 45° or more from the trend of the De Mille Fault. The overall smaller size of clasts in the southwestern part of the fan complex (bearing Mount Lowe clasts) is consistent with a general west-southwesterly sediment transport direction. This suggests a beheaded alluvial fan complex that originally crossed the fault and was fed from the east or northeast. No confirmation of such evidence at other more western sites close to the fault is possible because of limited access and lack of exposures of coarse-grained facies. Restoration of 34° of post-Saugus clockwise block rotation, as deduced from magnetic declination measurements made only about 7 km to the west-southwest (Levi and Yeats, 2003), suggests that the trend of sediment transport in upper Gold Canyon may have been more perpendicular than parallel to the De Mille Fault trend (fig. 10).

Fault Truncation of Clast Lithofacies Boundary

An approximate clast lithofacies boundary between Saugus Formation outcrops with and without Mount Lowe intrusive suite clasts is shown in figure 10*B*. This boundary separates two differently sourced parts of a beheaded alluvial fan complex. Mount Lowe clasts occur at Saugus Formation locality 16 but are absent at locality 51, both sites adjacent to the Watt Fault. Location 3 (figs. 10 and 7) is the midpoint between these localities. A possible trend of the boundary southward away from the fault is problematic because of Saugus Formation depositional facies changes, possibly influenced by the paleotopography during Saugus deposition. The boundary might trend southwestward before curving more westwardly on the distal part of the fan complex. This clast lithofacies change along the trend of the adjacent Watt and De Mille Faults also supports a sediment transport direction that is more perpendicular than parallel to the De Mille Fault.

Relative Abundances of Clast Types

Saugus Formation clasts derived from the anorthosite-syenite complex are more widely distributed, and more abundant, than more durable but better rounded Mount Lowe intrusive suite clasts where both occur together (appendix 1, table 2). At a few places, anorthosite clasts are absent; at a few

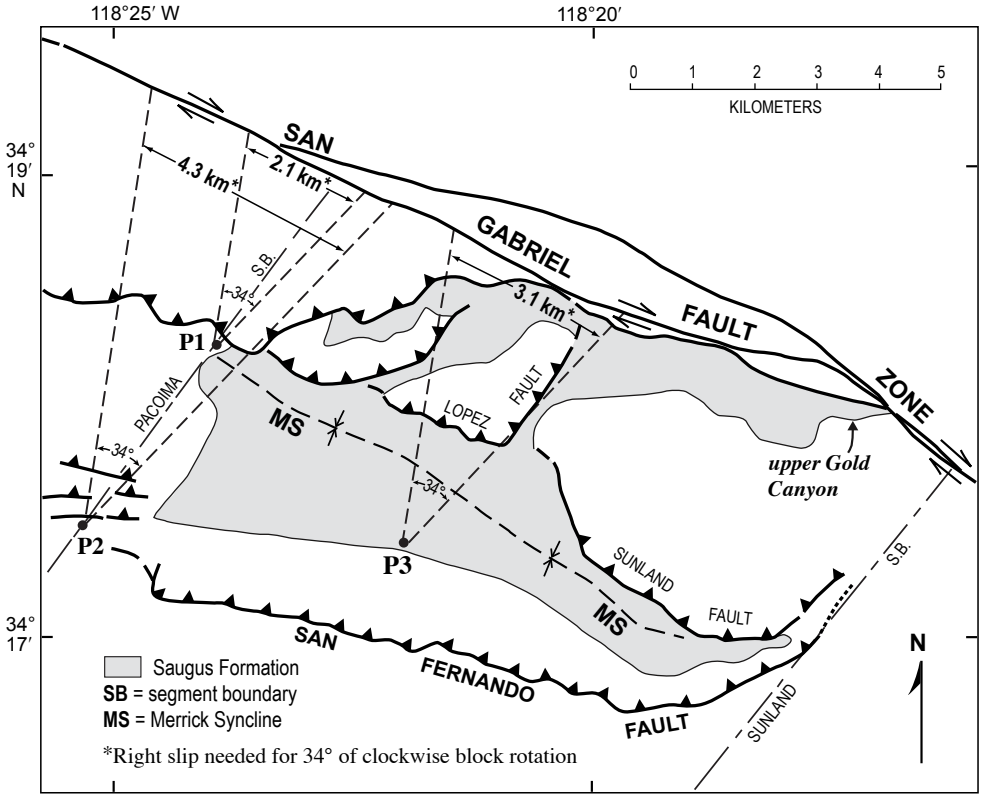

Figure 8. The "Merrick Syncline domain" local tectonic block between Pacoima Wash and Big Tujunga Canyon that is bounded by the "Sunland and Pacoima segment boundaries," the San Gabriel Fault Zone, and probably the San Fernando Fault Zone (adapted and modified from Levi and Yeats, 2003, fig. 11). Thirty-four degrees of clockwise block rotation about hypothetical vertical pivot point P1, P2, or P3 correspond to 2.1, 4.3, or 3.1 km of right-slip on the San Gabriel Fault Zone, respectively, if all block rotation is due to perfectly coupled rotational torque generated by De Mille Fault right slip.

Figure 9. Outcrops of Saugus Formation rocks. *A*, Fanglomerate exposed on the north wall of upper Gold Canyon about 250 m upstream from outcrops of Gold Canyon beds. *B*, Polymictic boulder bed exposed further upstream at locality 5 (fig. 10 and appendix 1, table 2). Anorthosite and marginal facies Mount Lowe intrusive suite clasts as large as 46 cm are common but are not the dominant or largest clast types. Hammer in white circle is 32 cm long.

others they constitute the entire clast population (Oakeshott, 1958, p. 84, 105; Weber, 1982, plate 2, locality 125; appendix 1, table 2). Intermittent flooding from different source areas can explain such differences. The predominance of anorthosite and leucogabbro clasts suggests that the principal source region was the south-central and eastern parts of the complex, where such rock types are most abundant (Carter, 1982, p. 10) (fig. 7). A small angular cobble composed of magnetite and hornblende from a northeastern Saugus Formation outcrop (fig. 10*A*, locality 9) is probably from one of many "titaniferous magnetite bodies" in the south-central and eastern part of the complex (Oakeshott, 1946, p. 245 and plate XXV; also "fgb"unit, Dibblee, 2002a, 2002b). All evidence is compatible with sources of the anorthosite clasts north or northeast of the San Gabriel Fault. Principal mapped Mount Lowe intrusive suite outcrops are far to the northeast (area of locations 4 on fig. 7). A notable exception is Mount Lowe rocks (without anorthosite) exposed in a much smaller area south of the San Gabriel Fault Zone east of its bifurcation, in the drainage area of the Clear Creek tributary of Big Tujunga Canyon (location 5 on fig. 7).

Summary

The large variety of rock types and degrees of rounding of most clasts in the very coarse-grained Saugus Formation facies (fig. 9) indicates a variety of source areas at various distances. Interbedded debris-flow and fluviatile beds indicate transportation and deposition by a river or large stream system with strong seasonal flow fluctuations. This relatively large drainage system was similar to the present upper Big Tujunga drainage basin north of the San Gabriel Fault Zone (fig. 7). The arithmetic mean of the largest dimension of the largest five subrounded to rounded Mount Lowe clasts in the Saugus Formation, all located in the upper Gold Canyon-Gold Canyon Saddle area, is 54 cm. Decrease of Mount Lowe clast size versus distance downstream from source outcrops was determined in modern gravels in Arroyo Seco (Krumbein, 1942, p. 1380-1382). We supplemented those data with observations of subangular to subrounded Mount Lowe boulders up to 1 m in size in Arroyo Seco gravels at the Vasquez Creek Fault crossing. Assuming the stream gradient of the present upper Big Tujunga Canyon, which is less than half that of Arroyo Seco above its intersection with the Vasquez Creek Fault, these data suggest that the 54-cm largest Mount Lowe clasts in the Saugus Formation in upper Gold Canyon were transported 16 km or more from their source outcrops. This in turn suggests that Saugus Formation Mount Lowe clasts might have eroded from the extensive source outcrops located north of the San Gabriel Fault in the eastern part of the upper Big Tujunga Canyon drainage system (area of locations 4 on fig. 7).

Quantifying post-Saugus Formation right slip on the De Mille-Vasquez Creek Faults is problematic because no trustworthy cross-fault tie is established. Saugus Formation is not found on the block between the Watt and Dillon Faults (Hill, 1930, p. 148; Oakeshott, 1958, p. 93) (fig. 2*A*). We are unaware of any perched remnant outcrops of Saugus Formation north of either the San Gabriel or Vasquez Creek Faults to the north and east. No Mount Lowe debris is found in south-directed tributaries to the 5-km-long Big Tujunga Canyon segment southeast of Gold Canyon. It is not known how far eastward the Saugus Formation strata south of the De Mille Fault in Gold Canyon originally extended. Parts of the easternmost Saugus Formation have been eroded, because the partly stratified beds, although very coarse grained and containing debris-flow deposits, also contain fine-grained fluviatile beds and are not proximal fan head deposits (fig. 9). The fan is now beheaded and eroded. Similarly, the original extent of the beheaded coalesced fan complex implied by the truncated boundary separating Saugus Formation with and without Mount Lowe clasts is unknown. Nevertheless, the cross-fault sources of Mount Lowe clasts are interpreted as being closer to the Little Tujunga Canyon-Gold Canyon area during Saugus Formation deposition than they are today. This is based on the more perpendicular than parallel transport direction of Saugus sediments across the Watt and De Mille Faults (after back-rotation), together with the location along the Watt Fault of the boundary of Saugus Formation with and without Mount Lowe clasts (location 3 on fig. 10). However, lacking correlatable piercing points, we cannot rule out some unknown amount of intervening fault-parallel sediment transport and therefore cannot offer conclusive measures of post-Saugus Formation right slip.

The hypothetical 2.1-4.3 km right separation based on post-Saugus Formation block rotation (fig. 8) is similar to a 4±2 km estimate derived from a mean slip rate of 2.3 mm/yr. (The mean slip rate is based on fault displacement beginning at the ca. 5.2±0.3 Ma age of the Gold Canyon beds, our post-beds right separation estimate of 12±2 km, and the 2.6 to 0.8 Ma estimated age of the Saugus Formation.) Lastly, the westernmost confirmed Mount Lowe intrusive suite clasts in the Saugus Formation adjacent to the Watt Fault are about 5.5 km (measured along the De Mille Fault) from the present Big Tujunga Canyon (locations 3 to 6 on fig. 7). Although none of these numbers lead to measures of right separation, the multiple lines of circumstantial evidence are consistent with 4 ±2 km as a reasonable estimate of post-Saugus Formation right separation on the combined De Mille-Vasquez Creek Faults.

Conclusions

Strands of the San Gabriel Fault Zone cut both the Gold Canyon beds and unconformably overlying Saugus Formation fanglomerate in upper Gold Canyon. Evidence from these rock units leads to several inferences concerning the onset age and amount of post-Miocene right separation on the combined De Mille-Vasquez Creek Faults: (1) Dating of macrofossil shell carbonates from the Gold Canyon beds using $^{87}Sr/^{86}Sr$ indicates marine deposition at 5.2±0.3 Ma. This maximum age for early right slip on the De Mille-Vasquez Creek faults refines the independently estimated "<7 and >3.7 Ma" onset

age (McCulloh and others, 2001, p. 22, 24). (2) Large angular Mount Lowe intrusive suite boulders in the Gold Canyon beds, eroded from cross-fault sources now separated from the beds by faults, indicate right separation of as much as 12±2 km on the De Mille-Vasquez Creek Faults. This conclusion is similar to an 11-km estimate (Ehlig, 1975b, p. 14) and a 12-13-km estimate based on multiple independent facts and separate reasoning (McCulloh and others, 2001). (3) At the San Gabriel Fault bifurcation, the hypothesized right separation on the Vasquez Creek Fault joins 22-23 km of middle-late Miocene right separation (Ehlig, 1968) of the San Gabriel Fault. Right separation of as much as 34-35 km west of the bifurcation passes northwestward along the fault beyond the San Gabriel Mountains. (4) Saugus Formation clast sizes and lithologic

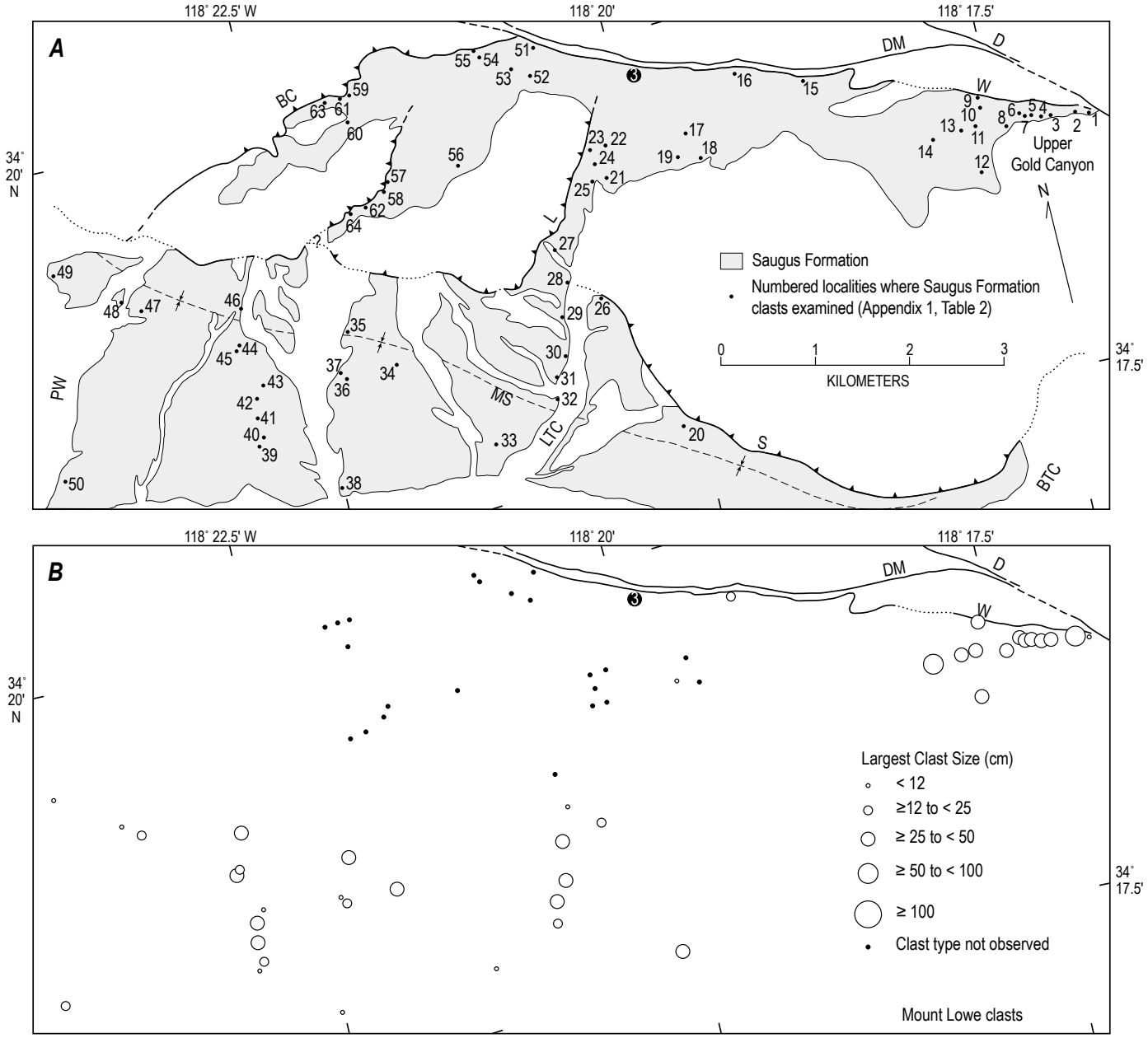

Figure 10. Distribution of maximum clast sizes and bed-forming processes of the Saugus Formation. Fault and geographic labels are as in figures 1 and 2. *A*, Simplified geologic map showing major faults and most of the mapped Saugus Formation between Pacoima Wash and upper Gold Canyon, with numbered localities where maximum sizes of Saugus Formation clasts were measured (appendix 1, table 2). Older and younger bordering units (see fig. 2) are not differentiated here. *B*, Distribution of largest Mount Lowe clasts and sites where Mount Lowe clasts are absent. *C*, Distribution of largest clasts of all rock types. *D*, Distribution of dominant bed-forming process. White-on-black circle 3 (shown in *A, B, D,* and fig. 7) is the approximate location of the boundary between Saugus Formation outcrops adjacent to the Watt Fault with and without Mount Lowe intrusive suite clasts, chosen midway between localities 16 and 51.

proportions in the Gold and Little Tujunga Canyons indicate cross-fault clast sources to the north and northeast, sediment transport more nearly transverse than parallel to the present De Mille Fault strike, and transport distances 16 km or more for Mount Lowe clasts. These interpretations, combined with a fault-coupled local block-rotation hypothesis and a right-slip rate estimate of 2.3 mm/yr on the De Mille-Vasquez Creek Faults since 5.2 Ma, suggests that post-Saugus Formation (< 2.6 to 0.78 Ma) right separation is 4±2 km on the De Mille-Vasquez Creek Faults.

The age of 5.2±0.3 Ma (earliest Pliocene) for the Gold Canyon beds indicates that they are equivalent to either youngest Towsley Formation or oldest Pico Formation. The depositional environment and fauna of the beds suggest kinship with the basal part of the Pico Formation.

Establishing the age of the Gold Canyon beds and correlating them to more completely studied sections in regions to the south and west of the western San Gabriel Mountains required a comprehensive regional stratigraphic and geochronologic framework. This study produced several added results: (1) Large and abrupt changes in stratal thicknesses (or disconformity gaps) of this basin-margin setting are documented. (2) This is the first published account of fossil oyster spat, associated with deep marine benthic foraminifers and planktonic calcareous nannofossils and diatoms, in this area; they are found at two stratigraphically and geographically separated Modelo

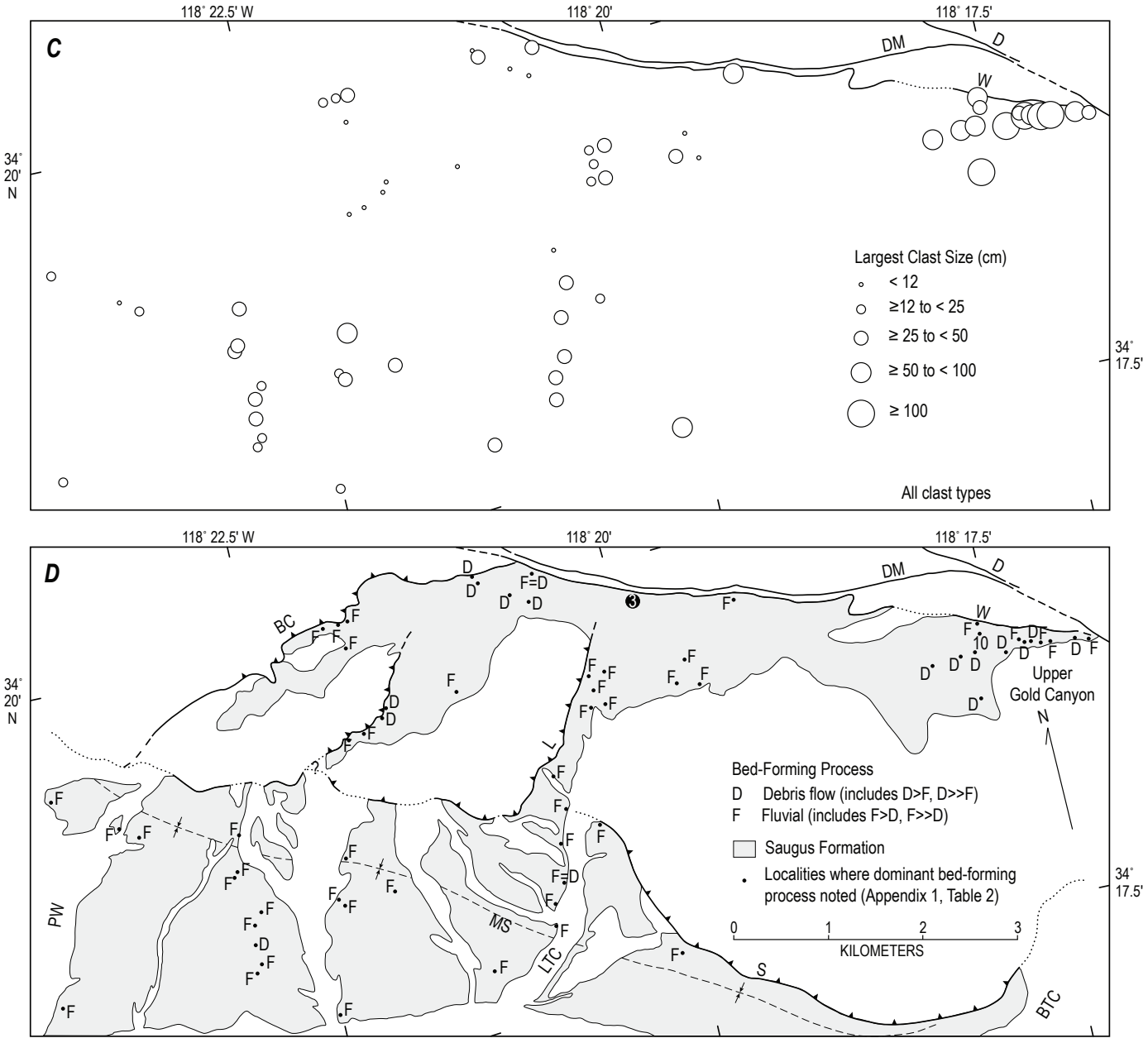

Figure 10.—Continued.

Formation exposures. This unusual assemblage indicates an exceptional nearshore, but deep-water, upwelling marine setting. (3) Connection from the shallow marine Gold Canyon beds to more open marine settings probably extended south or southwest from Gold Canyon. Presumably correlative beds, lithologically dissimilar and largely nonfossiliferous, are just east of Pacoima Wash. Facies differences and both erosion and burial, probably before and also after deposition of the Saugus Formation, obscured or destroyed direct evidence of the 5.2-Ma tidal connection, the existence of which is suggested today only by the presence of the isolated Gold Canyon beds.

Acknowledgments

We thank D.M. Morton, J.C. Matti, and the U.S. Geological Survey Bradley Scholar Program for material support. We are especially grateful to the University of Texas at Dallas for crucial support; N.R. Miller provided ICP analyses of fossil carbonate samples. We are grateful to J.G. Vedder and C.L. Powell, II, who examined several molluscan assemblages and discussed their living environments. R.E. Powell, A.P. Barth, B.A. Carter, J.A. Nourse, and R.L. Squires helpfully responded to questions about their work in the region. J.D. Stock discussed alluvial processes with the senior author. Harry Filkorn provided lists of archived invertebrate fossils from the area. G.J. Saucedo furnished us with unpublished geologic maps of two areas. Steve Bear and John Keeler (Angeles National Forest, U.S. Forest Service) provided crucial access to the field area. The Wildlife Way Station and the Middle Ranch allowed entry to their lands. Sterling Klappell (Los Angeles County Public Works Department) provided Big Tujunga Canyon stream flow information and control that facilitated fieldwork. Two reviews each by R.E. Powell and D.M. Morton provided critical guidance, and reviews by P. Stone, J.T. Tinsley, and J.G. Vedder, were important. Zenon Valin and Peter Triezenberg prepared the figures. Nardia Beyer kindly accompanied the senior author during eight field days in Gold Canyon and surrounding areas.

References

Allen, C.R., Hanks, T.C., and Whitcomb, J.H., 1975, Seismological studies of the San Fernando earthquake and their tectonic implications, Chapter 20 *of* Oakeshott, G.B., ed., San Fernando, California, earthquake of 9 February 1971: California Division of Mines and Geology Bulletin 196, p. 257-262.

Backman, J., and Raffi, I., 1997, Calibration of Miocene nannofossil events to orbitally tuned cyclostratigraphies from Ceara Rise: Proceedings of the Ocean Drilling Program, Scientific Results, v. 154, p. 83-99.

Barron, J.A., 1981, Late Cenozoic diatom biostratigraphy and paleoceanography of the middle-latitude eastern North Pacific, Deep Sea Drilling Project Leg 63, *in* Yeats, R.S., Haq, B.U., and others, eds., Initial reports of the Deep Sea Drilling Project, v. 63, Washington, D. C., U.S. Government Printing Office, p. 507-538.

Barron, J.A., 1986a, An updated diatom biostratigraphy for the Monterey Formation of California, *in* Casey, R.G., and Barron, J.A., eds., Siliceous microfossils and microplankton studies of the Monterey Formation and its modern analogues: Pacific Section, Society of Economic Paleontologists and Mineralogists, Special Publication, Book 45, p. 105-119.

Barron, J.A., 1986b, Paleoceanographic and tectonic controls on deposition of the Monterey Formation and related siliceous rocks in California: Palaeogeography, Palaeoclimatology, Palaeoecology, Symposium Volume, v. 27, p. 27-45.

Barron, J.A., 2003. Appearance and extinction of planktonic diatoms during the past 18 m.y. in the Pacific and Southern oceans: Diatom Research, v. 8, p. 203-224.

Barron, J.A., and Gladenkov, A.Y, 1995, Early Miocene to Pleistocene diatom stratigraphy of Leg 145, *in* Rea, D.K., Basov, I.A., Scholl, D.W., and Allan, J.F., eds., Proceedings of Ocean Drilling Program, Scientific Results, v. 145, p. 3-19.

Barron, J.A., and Isaacs, C.M., 2001, Updated chrononstratigraphic framework for the California Miocene, *in* Isaacs, C.M., and Rullkotter, J., eds., The Monterey Formation—from rocks to Molecules: Columbia University Press, New York, 393-395.

Barrows, A.G., Kahle, J.E., Saul, R.B., and Weber, F.J., Jr., 1974, Geologic map of the San Fernando earthquake area, *in* Oakshott, G.B., ed., San Fernando, California, earthquake of 9 February 1971: California Division of Mines and Geology Bulletin 196, plate 2, map scale 1:18,000.

Barth, A.P., and Ehlig, P.L., 1988, Geochemistry and petrogenesis of the marginal zone of the Mount Lowe intrusion, central San Gabriel Mountains, California: Contributions to Mineralogy and Petrology, v. 100, p. 192-204.

Barth, A.P., Tosdal, R.M., and Wooden, J.L., 1990, A petrologic comparison of Triassic plutonism in the San Gabriel and Mule Mountains, southern California: Journal of Geophysical Research, v. 95, n. B12, p. 20075-20096.

Barth, A.P., Wooden, J.L., Tosdal, R.M., and Morrison, J., 1995, Crustal contamination in the petrogenesis of a calc-alkalic rock series; Josephine Mountain intrusion, California: Geological Society of America Bulletin, v. 107, p. 201-212.

Barth, A.P., Wooden, J.L., and Coleman, D.S., 2001, SHRIMP-RG U-Pb zircon geochronology of Mesoproterozoic metamorphism and plutonism in the southwesternmost United States: Journal of Geology, v. 109, p. 319-327.

Blake, G.H., 1991, Review of the Neogene biostratigraphy and stratigraphy of the Los Angeles basin and implications for basin evolution, *in* Biddle, K.T., ed., Active margin basins: American Association of Petroleum Geologists Memoir 52, 135-184.

Brand, Uwe, and Veizer, Jan, 1980, Chemical diagenesis of a multicomponent carbonate system—1. Trace elements: Journal of Sedimentary Petrology, v. 50, p. 1219-1236.

Burke, W.H., Denison, R.E., Hetherington, E.A., Koepnick, R.B., Nelson, H.F., and Otto, J.B., 1982, Variation of seawater $^{87}Sr/^{86}Sr$ throughout Phanerozoic time: Geology, v. 10, p. 520-523.

Carter, Bruce, 1982, Geology and structural setting of the San Gabriel anorthosite-syenite body and adjacent rocks of the western San Gabriel Mountains, Los Angeles County, California: Geological Society of America, Cordilleran Section, Field Trip Number 5; Geologic excursion in the Transverse Ranges, Southern California, Guidebook, p. 1-53.

Carter, Bruce, and Silver. L.T., 1972, Structure and petrology of the San Gabriel anorthosite-syenite body, California: Twenty-fourth International Geological Congress, section 2, Montreal, Canada, p. 303-331.

Crook, Richard, Jr., Allen, C.R., Kamb, Barclay, Payne, C.M., and Proctor, R.J., 1987, Quaternary geology and seismic hazard of the Sierra Madre and associated faults, western San Gabriel Mountains, *in* Recent reverse faulting in the Transverse Ranges, California: U.S. Geological Survey Professional Paper 1339, p. 27-63, plates 2.1-2.6, map scale 1:24,000.

Crouch, J.K., 1979. Neogene tectonic evolution of the California Continental Borderland and western Transverse Ranges: Geological Society of America Bulletin, v. 90, p. 338-345.

Crowell, J.C., 2003, Tectonics of Ridge Basin region, southern California, *in* Crowell, J. C., ed., Evolution of Ridge Basin, southern California; an interplay of sedimentation and tectonics: Geological Society of America Special Paper 367, p. 157-203.

Crowell J.C., and Walker, J.W.R., 1962, Anorthosite and related rocks along the San Andreas Fault Southern California: University of California Publications in Geological Sciences, v. 40, no. 4, p. 219-288.

Denison, R.E., Koepnick, R.B., Fletcher, A., Howell, M.W., and Calloway, W.S., 1994, Criteria for the retention of original seawater $^{87}Sr/^{86}Sr$ in ancient shelf limestones: Chemical Geology, v. 112, p. 131-143.

Dibblee, T.W., Jr., 1968, Displacement on the San Andreas fault system in the San Gabriel, San Bernardino and San Jacinto Mountains, southern California, *in* Dickinson, W.R., and Grantz, Arthur, eds., Proceedings of conference on geologic problems of San Andreas fault system: Stanford University Publications in Geological Sciences, v. XI, p. 260-278.

Dibblee, T.W., Jr., 1982, Geology of the San Gabriel Mountains, Southern California, *in* Fife, D. L., and Minch, J.A., eds., Geology and mineral wealth of the California Transverse Ranges: South Coast Geological Society, Inc., Santa Ana, California, Annual Symposium and Guidebook Number 10, p. 131-147.

Dibblee, T.W., Jr., 1989, Geologic map of the Pasadena quadrangle, Los Angeles County, California: Santa Barbara, California, Dibblee Geological Foundation Map #DF-23, map scale 1:24,000.

Dibblee, T.W., Jr., 1991a, Geologic map of the San Fernando and Van Nuys (north 1/2) quadrangles, Los Angeles County, California: Santa Barbara, California, Dibblee Geological Foundation Map #DF-33, map scale 1:24,000.

Dibblee, T.W., Jr., 1991b, Geologic map of the Sunland and Burbank (north 1/2) quadrangles, Los Angeles County, California: Santa Barbara, California, Dibblee Geological Foundation Map #DF-32, map scale 1:24,000.

Dibblee, T.W., Jr., 1992, Geologic map of the Oat Mountain and Canoga Park (North 1/2) quadrangles, Los Angeles County, California: Santa Barbara, California, Dibblee Geological Foundation Map #DF-36, map scale 1:24,000.

Dibblee, T.W., Jr., 2002a, Geologic map of the Condor Peak quadrangle, Los Angeles County, California: Santa Barbara, California, Dibblee Geological Foundation Map #DF-84, map scale 1:24,000.

Dibblee, T.W., Jr., 2002b, Geologic map of the Chilao Flat quadrangle, Los Angeles County, California: Santa Barbara, California, Dibblee Geological Foundation Map #DF-85, map scale 1:24,000.

Ehlig, P.L., 1968, Displacement along the San Gabriel Fault, San Gabriel Mountains, Southern California, *in* Abstracts for 1966: Geological Society of America Special Paper 101, p. 60.

Ehlig, P.L., 1975a, Basement rocks of the San Gabriel Mountains, south of the San Andreas Fault, southern California, *in* Crowell, J.C., ed., San Andreas Fault in Southern California: California Division of Mines and Geology Special Report 118, p. 177-185.

Ehlig, P.L., 1975b, Geologic framework of the San GabrielMountains, *in* Oakshott, G.B., ed., San Fernando, California, earthquake of 9 February 1971, California Division of Mines and Geology Bulletin 196, p. 7-18.

Ehlig, P.L., 1981, Origin and tectonic history of the basement terrane of the San Gabriel Mountains, central Transverse Ranges, *in* Ernst, W.G., ed., The geotectonic development of California (Rubey Volume I): Englewood Cliffs, New Jersey, Prentice-Hall, p. 253-283.

Finger, K.L., 1990, Atlas of California Neogene foraminifera: Cushman Foundation for Foraminifera Research, Special Publication 28, 271 p.

Fleck, R.J., Sutter, J.F., and Elliot, D.H., 1977, Interpretation of discordant $^{40}Ar/^{39}Ar$ age spectra of Mesozoic tholeiites from Antarctica: Geochimica et Cosmochimica Acta, v. 41, p. 15-32.

Flores, J.-A., Sierro, F.J., Filippelli, G.M., Bárcena, M.A., Pérez-Folgado, M., Vázquez, A., Utrilla, R., 2005, Surface water dynamics and phytoplankton communities during deposition of cyclic late Messinian sapropel sequences in the western Mediterranean: Marine Micro-paleontology, v. 56, p. 50-79.

Fornaciari, Eliana, 2000, Calcareous nannofossil biostratigraphy of the California margin: Proceedings of the Ocean Drilling Program, Scientific Results, v. 167, p. 3-40.

Higgs, D.V., 1954, Anorthosite and related rocks of the western San Gabriel Mountains, Southern California: University of California Publications in Geological Sciences, v. 30, p. 171-222.

Hill, M.L., 1930, Structure of the San Gabriel Mountains, North of Los Angeles, California: University of California Publications in Geological Sciences, v. 19, p. 137-163, map scale 1:36,555.

Hoots, H.W., 1931, Geology of the eastern part of the Santa Monica Mountains, Los Angeles County, California: U.S. Geological Survey Professional Paper 165-C, p. 83-134, map scale, 1:24,000.

Hornafius, J.S., Luyendyk, B.P., Terres, R.R., and Kamerling, M.J., 1986, Timing and extent of Neogene tectonic rotation in the western Transverse Ranges, California: Geological Society of America Bulletin, v. 97, p. 1476-1487.

Hoskins, E.G., and Griffiths, J.R., 1971, Hydrocarbon potential of northern and central California offshore, *in* Cram, I.H., ed., Future petroleum provinces of the United States—their geology and potential: American Association of Petroleum Geologists Memoir 15, p. 212-228.

Howarth, R.J., and McArthur, J.M., 1997, Statistics for strontium isotope stratigraphy; a robust LOWESS fit to the marine Sr-isotope curve for 0 to 206 Ma, with look-up table for derivation of numeric age: Journal of Geology, v. 105, p. 441-456.

Huftile, G.J., and Yeats, R.S., 1996, Deformation rates across the Placerita (Northridge M_W = 6.7 aftershock zone) and Hopper Canyon segments of the western Transverse Ranges deformation belt: Bulletin of the Seismological Society of America, v. 86, n. 1B, p. S3-S18.

Jennings, C.W., 1977, Geologic map of California: California Geologic Data Map Series, California Division of Mines and Geology, scale 1:750,000.

Joseph, S.E., Criscione, J.J., Davis, T.E., and Ehlig, P.L., 1982, The Lowe igneous pluton, *in* Fife, D.L., and Minch, J.A., eds., Geology and mineral wealth of the California Transverse Ranges: South Coast Geological Society, Inc., Santa Ana, California, Annual Symposium and Guidebook Number 10, p. 307-309.

Kahle, J.E., 1975, Surface effects and related geology of the Lakeview fault segment of the San Fernando Fault Zone, *in* Oakeshott, G.B., ed., San Fernando, California, earthquake of 9 February 1971: California Division of Mines and Geology Bulletin 196, Chapter 8, p. 119-135.

Kew, W.S.W., 1924, Geology and oil resources of a part of Los Angeles and Ventura Counties, California: U.S. Geological Survey Bulletin 753, 202 p, 2 plates, map scale 1:62,500.

Krumbein, W.C., 1942, Flood deposits of Arroyo Seco, Los Angeles County, California: Geological Society of America Bulletin, v. 53, p. 1355-1402.

Lee, Hee-Kwon, and Schwarcz, H.P., 1996, Electron spin resonance plateau dating of periodicity of activity on the San Gabriel Fault Zone, southern California: Geological Society of America Bulletin, v. 108, p. 735-746.

Levi, Shaul, and Yeats, R.S., 1993, Paleomagnetic constraints on the initiation of uplift on the Santa Susana Fault, western Transverse Ranges, California: Tectonics, v. 12, p. 688-702.

Levi, Shaul, and Yeats, R.S., 2003, Paleomagnetic definition of crustal fragmentation and Quaternary block rotations in the east Ventura Basin and San Fernando valley, southern-California: Tectonics, v. 22, p. 15-1-15-16.

Levi, Shaul, Nabelek, John, and Yeats, R.S., 2005, Paleomagnetism-based limits on earthquake magnitudes in northwestern metropolitan Los Angeles, California, USA: Geology, v. 33, p. 401-404.

Lorio, W.J., and Malone, Sandra, 1994, The cultivation of American oysters: Southern Regional Aquaculture Center Publication No. 432, 8 p.

Lourens, L.J., Hilgen, J., Laskar, F.J., Shackleton, N.J., and Wilson, D., 2004, The Neogene period, *in* Gradstein, F., Ogg, J., and Smith, A., eds., A geologic time scale 2004, New York, Cambridge University Press, p. 409-440.

Margalef, R. 1978, Life-forms of phytoplankton as survival alternatives in an unstable environment: Oceanologica Acta, v. 1, p. 493-509.

Matti, J.C., and Morton, D.M., 1993, Paleogeographic evolution of the San Andreas Fault in Southern California; a reconstruction based on a new cross-fault correlation, *in* Powell, R.E., Weldon, R.J., II, and Matti, J.C., eds., The San Andreas fault system; displacement,palinspastic reconstruction, and geologic evolution: Geological Society of America Memoir 178, p. 107-159.

McArthur, J.M., and Howarth, R.J., 2004, Strontium isotope stratigraphy, *in* Gradstein, F.M., Ogg, J.G., and Smith, A.G., eds., A geologic time scale 2004: New York, Cambridge University Press, p. 96-105.

McArthur, J.M., Howarth, R.J., and Bailey, T.R., 2001, Strontium isotope stratigraphy; LOWESS Version 3; best fit to the marine Sr-isotope curve for 0-509 Ma and accompanying look-up table for deriving numerical age: Journal of Geology, v. 109, p. 155-170.

McCulloh, T.H., Beyer. L.A., and Enrico, R.J., 2000, Paleogene strata of the eastern Los Angeles basin, California; paleogeography and constraints on Neogene structural evolution: Geological Society of America Bulletin, v. 112, p. 1155-1178.

McCulloh, T.H., Beyer, L.A., and Morin, R.W., 2001, Mountain Meadows Dacite; Oligocene intrusive complex that welds together the northwestern Peninsular Range, central Transverse Ranges and Los Angeles Basin, California: U.S. Geological Survey Professional Paper 1649. 34 p.

McCulloh, T.H., Fleck, R.J., Denison, R.E., Beyer, L.A., and Stanley, R.G., 2002, Age and tectonic significance of volcanic rocks in the northern Los Angeles Basin, California: U.S. Geological Survey Professional Paper 1669, 24 p.

McIntyre, G.A., Brooks, C., Compston, W., and Turek, A., 1966, The statistical assessment of Rb-Sr isochrons: Journal of Geophysical Research, v. 71, p. 5459-5468.

Merifield, P.M., 1958, Geology of a portion of the southwestern San Gabriel Mountains, San Fernando and Oat Mountains Quadrangles, Los Angeles County, California: University of California, Los Angeles, Masters thesis, 61 p., map scale 1:12,000.

Merrihue, Craig, and Turner, Grenville, 1966, Potassium-argon dating by activation with fast neutrons: Journal of Geophysical Research, v. 71, p. 2852-2857.

Miller, W.J., 1934, Geology of the western San Gabriel Mountains of California: Publications of the University of California at Los Angeles in Mathematical and Physical Sciences, v. 1, p. 1-114.

Morton, D.M., 1973, Geology of parts of the Azusa and Mount Wilson quadrangles, San Gabriel Mountains, Los Angeles County, California: California Division of Mines and Geology Special Report 105, 21 p., 2 plates, map scale 1:12,000.

Morton, D.M., 1975, Synopsis of the geology of the eastern San Gabriel Mountains, southern California, *in* Crowell, J. C., ed., San Andreas fault in southern California: California Division of Mines and Geology Special Report 118, p. 170-176.

Morton, D.M, and Miller F.K., 2003, Preliminary geologic map of the San Bernardino 30' X 60' quadrangle, California: U.S. Geological Survey Open-File Report 03-293, 5 sheets, scale 1:100,000

Nourse, J.A., 2002, Middle Miocene reconstruction of the central and eastern San Gabriel Mountains, southern California, with implications for evolution of the San Gabriel Fault and Los Angeles basin, *in* Barth, A., ed., Contributions to crustal evolution of the south-western United States: Geological Society of America Special Paper 365, p. 161-185.

Oakeshott, G.B., 1946, Titaniferous iron-ore deposits of the western San Gabriel Mountains, Los Angeles County, California, *in* Iron resources of California, California Division of Mines, Bulletin 129, Part P, p. 245-266, map scales 1:190,000 and 1:48,000.

Oakeshott, G.B., 1958, Geology and mineral deposits of San Fernando Quadrangle, Los Angeles County, California: California Division of Mines and Geology Bulletin 172, p. 147

Oakeshott, G.B., 1975, Geology of the epicental area, chapter 3 *of* Oakeshott, G. B., ed., San Fernando, California, earthquake of 9 February 1971: California Division of Mines and Geology, Bulletin 196, p. 19-30.

Okada, H., and Bukry, D., 1980, Supplementary modification and introduction of code numbers to the low-latitude coccolith biostratigraphic zonation (Bukry, 1973; 1975): Marine Micropaleontology, v. 5, p. 321-325

Perch-Nielsen, K., 1985, Mesozoic calcareous nannofossils, Cenozoic calcareous nannofossils, *in* Bolli, H.M., Saunders, J.B., and Perch-Nielsen, K., eds., Plankton Stratigraphy: Cambridge University Press, p. 329-554.

Powell, R.E., 1993, Balanced palinspastic reconstruction of pre-late Cenozoic paleogeology, southern California; geologic and kinematic constraints on evolution of the San Andreas fault system, *in* Powell, R.E., Weldon, R.J., II, and Matti, J.C., eds., The San Andreas fault system; displacement, palinspastic reconstruction, and geologic evolution: Geological Society of America Memoir 178, p. 1-106.

Powell, R.E., and Weldon, R.J., II, 1992, Evolution of the San Andreas Fault: Annual Reviews of Earth and Planetary Sciences, v. 20, p. 431-468.

Powell, R.E., Cox, B.F., Matti, J.C., and Gabby, P.N., 1983, Mineral resource potential of the Arroyo Seco roadless area, Los Angeles County, California: U.S. Geological SurveyMiscellaneous Field Studies Map MF 1607-A, 7 p., 1 plate, scale 1:24,000.

Samson, S.D., and Alexander, E.C., 1987, Calibration of the interlaboratory $^{40}Ar/^{39}Ar$ dating standard, MMhb-1: Chemical Geology (Isotope Geoscience Section), v. 66, p. 27-34.

Saul, R.B., 1975, Geology of the southeast slope of the Santa Susana Mountains and geologic effects of the San Fernando earthquake, chapter 5 *of* Oakeshott, G.B., ed., San Fernando, California, earthquake of 9 February 1971: California Division of Mines and Geology Bulletin 196, p. 53-70.

Saul, R.B., 1976, Geology of the west central part of the Mt. Wilson quadrangle, San Gabriel Mountains, Los Angeles County, California: California Division of Mines and Geology Map Sheet 28, map scale 1:12,000.

Saul, R.B., and Wootton, T.M., 1983, Geology of the south half of the Mint Canyon quadrangle, Los Angeles County, California: California Division of Mines and Geology Open-File Report 83-24LA, 139 p., 6 plates, map scale 1:9600.

Savage, J.C., Burford, R.O., and Kinoshita, W.T., 1975, Earth movements from geodetic measurements, chapter 8 *of* Oakeshott, G.B., ed., San Fernando, California, earthquake of 9 February 1971: California Division of Mines and Geology Bulletin 196, p. 175-186.

Scott, K.M., 1971, Origin and sedimentology of 1969 debris flows near Glendora, California, *in* Geological Survey Research 1971: U.S. Geological Survey Professional Paper 750-C, p. C242-C247.

Shelton, J.S., 1955, Glendora Volcanic rocks, Los Angeles basin, California: Geological Society of America Bulletin, v. 66, p. 45-89.

Silver, L.T., McKinney, C.R., Deutsch, S., and Bolinger, J., 1963, Precambrian age determinations in the western San Gabriel Mountains, California: Journal of Geology, v. 71, p. 196-214.

Smith, D.P., 1986, Geology of the north half of the Pasadena quadrangle, Los Angeles County, California: Division of Mines and Geology Open File Report 86-4 LA, 40 p, 2 plates, map scale 1:12,000.

Squires, R.L., Groves, L.T., and Smith, J.T., 2006, New information on molluscan paleontology and depositional environments of the upper Pliocene Pico Formation, Valencia area, Los Angeles County, southern California: Natural History Museum of Los Angeles County, Contributions in Science Number 511, 24 p.

Steiger, R.H., and Jager, E., 1977, Subcommission on geochronology; convention on the use of decay constants in geo- and cosmochronology: Earth and Planetary Science Letters, v. 36, p. 359-362.

Stitt, L.T., and Yeats, R.S., 1982, A structural sketch of the Castaic area, northeastern Ventura Basin and northern Soledad basin, California, *in* Fife, D.L., and Minch, J.A., eds., Geology and mineral wealth of the California Transverse Ranges: Santa Ana, California, South Coast Geological Society, Inc., p. 390-394.

Theodoridis, S., 1984, Calcareous nannofossil biozonation of the Miocene and revision of the helicoliths and discoasters: Utrecht Micropaleontological Bulletins, no. 32, 271 p.

Tsutsumi, Hiroyuki, and Yeats, R.S., 1999, Tectonic setting of the 1971 Sylmar and 1994 Northridge earthquakes in the San Fernando Valley, California: Bulletin of the Seismological Society of America, v. 89, p. 1232-1249.

Turner, D.L., 1970, Potassium-argon dating of Pacific Coast Miocene foraminiferal stages, *in* Bandy, O.L., ed., Radiometric dating and paleontologic zonation: Geological Society of America Special Paper 124, p. 91-129.

U. S. Geological Survey, 1971, Surface faulting, *in* The San Fernando, California, earthquake of February 9, 1971: U.S. Geological Survey Professional Paper 733, p. 55-76.

Weber, F.H., Jr., 1982, Geology and geomorphology along the San Gabriel Fault Zone, Los Angeles and Ventura Counties, California: California Division of Mines and Geology Open-File Report 82-2 LA, 157 p., 3 plates.

Weber, F.H., Jr., 1988a, Reinterpretation of structural elements and displacement history along the San Gabriel Fault between the San Andreas Fault and the westernmost San Gabriel Mountains, Los Angeles, Kern, and Ventura Counties, California, Part IV, Evaluation of activity of the San Gabriel Fault Zone, Los Angeles and Ventura Counties, California: Final Technical Report, Contract Number USGS 14-08-0001-21928, Modification 2, State of California, Department of Conservation, submitted October 15, 1998, 115 p.

Weber, F.H., Jr., 1988b, Geologic relationships along the San Gabriel Fault between Hardluck Canyon and Castaic: California Geology, v. 41, no. 10, p. 229-238.

Weigand, P.W., and Savage, K.L., 1993, Review of the petrology and geochemistry of the Miocene Conejo Volcanics of the Santa Monica Mountains, California, *in* Weigand, P.W., Fritsche, A.E., and Davis, G.E., eds., Depositional and volcanic environments of middle Tertiary rocks in the Santa Monica Mountains, southern California: Pacific Section, Society for Sedimentary Geology, Book 72, p. 93-112.

Weldon, R.J., II, Meisling, K.E., and Alexander, J., 1993, A speculative history of the San Andreas Fault in the central Transverse Ranges, California, *in* Powell, R.E., Weldon, R. J., II, and Matti, J.C., eds., The San Andreas Fault system; displacement, palinspastic reconstruction, and geologic evolution: Geological Society of America Memoir 178, p. 161-198.

Wentworth, C.M., and Yerkes, R.F., 1971, Geologic setting and activity of faults in the San Fernando area, California, *in* The San Fernando, California, earthquake of February 9, 1971: U.S. Geological Survey Professional Paper 733, p. 6-16.

Winterer E.L., and Durham, D.L., 1958, Geologic map of a part of the Ventura basin, Los Angeles County, California: U.S. Geological Survey Oil and Gas Investigations Map OM 196, map scale 1:24,000.

Winterer, E.L., and Durham, D.L., 1962, Geology of southeastern Ventura basin, Los Angeles County, California: U.S. Geological Survey Professional Paper 334-H, p. 274-366, 6 plates, map scale1:24,000.

Wright, T.L., 2001, Subsurface geology of the San Fernando Valley—a progress report, *in* Wright, T.L., and Yeats, R.S., eds., Geology and tectonics of the San Fernando Valley and east Ventura Basin, California: Bakersfield, California, Pacific Section American Association of Petroleum Geologists, p. 55-62.

Yeats, R.S., 1979, Stratigraphy and paleogeography of the Santa Susana Fault Zone, Transverse Ranges, California, *in* Armentrout, J.M., Cole, M.R., and TerBest, Harry, Jr., eds., Cenozoic paleogeography of the western United States: Pacific Section, Society of Economic Paleontologists and Mineralogists, Pacific Coast Paleography Symposium 3, Anaheim, California, p. 191-204.

Yeats. R.S., 1987, Late Cenozoic structure of the Santa Susana Fault Zone, *in* Recent reverse faulting in the Transverse Ranges, California: U.S. Geological Survey Professional Paper 1339, p. 137-160.

Yeats, R.S., 2001, Neogene tectonics of the east Ventura and San Fernando Basins, *in* Wright, T.L., and Yeats, R.S., eds., Geology and tectonics of the San Fernando Valley and east Ventura Basin, California; an overview: Bakersfield, California, American Association of Petroleum Geologists, Pacific Section, Guidebook GB 77, p. 9-36.

Yeats, R.S., 2004, Tectonics of the San Gabriel Basin and surroundings, southern California: Geological Society of America Bulletin, v. 116, p. 1158-1182.

Yeats, R.S., and Stitt, L.T., 2003, Ridge Basin and San Gabriel Fault in the Castaic lowland, southern California: Geological Society of America Special Paper 367, p. 131-156.

Yeats, R.S., Huftile, G.J., and Stitt, L.T., 1994, Late Cenozoic tectonics of the east Ventura basin, Transverse Ranges, California: American Association of Petroleum Geologists Bulletin, v. 78, p. 1040-1074.

Yerkes, R.F., and Campbell, R.H., 1979, Stratigraphic nomenclature of the central Santa Monica Mountains, Los Angeles County, California: U.S. Geological Survey Bulletin 1457-E, 31 p., 3 plates.

Yerkes, R.F., and Campbell, R.H., 2005, Preliminary geologic map of the Los Angeles 30’ X 60’ quadrangle, southern California, Version 1.0: U.S. Geological Survey Open-File Report 2005-1019, 51 p., 2 sheets, map scale 1:100,000.

Young J.R., 1998, Neogene, *in* Bown, P.R., ed., Calcareous nannofossil biostratigraphy: Chapman & Hall, British Micropalaeontology Society Series, p. 225-265.

Appendixes

Appendix 1. Description of Saugus Formation Clasts

Three suites of San Gabriel Mountain basement rocks vary in importance as sources of clasts in the Saugus Formation. The Late Triassic Mount Lowe intrusive suite is of primary importance and is predominantly a monzodioritic to granodioritic metaplutonic complex with distinctive marginal zone facies (Miller, 1934; Ehlig, 1975a, 1981; Joseph and others, 1982; Powell and others, 1983; Barth and Ehlig, 1988; Barth and others, 1990; Nourse, 2002). A Mesoproterozoic anorthosite-syenite complex is composed of distinctive anorthosite and leucogabbro plus lesser syenite, monzodiorite, gabbro, and "ultramafite" (Oakeshott, 1958; Crowell and Walker, 1962; Carter and Silver, 1972; Carter, 1982, p. 1). A Paleoproterozoic metasedimentary and metaigneous gneiss suite (Silver and others, 1963) includes the Mendenhall Gneiss (Oakeshott, 1958), distinctive retrograded quartzofeldspathic granulites, some containing rutile-bearing clear or distinctively colored lavender or blue quartz, (Higgs, 1954; Oakeshott, 1958; Crowell and Walker, 1962; Barth and others, 1995; A.P. Barth, oral commun., 2005), and mafic granulite. Amphibolite facies layered and augen gneiss, and some aluminous schist (Silver and others, 1963; Ehlig, 1975a, 1981; Powell and others, 1983; Barth and others, 1995, 2001; Nourse, 2002) are among other Paleoproterozoic gneissic rock types. Outcrop areas of these suites are shown in figure 7.

Table 2 records maximum length and degree of rounding of distinctive clasts of Mount Lowe intrusive suite lithologies and anorthosite or leucogabbro clasts at 63 localities numbered from east to west in figure 10. The maximum dimension of all clasts is also tabulated. Massive dioritic to granitic plutonites and associated rock types dominate clast populations at most Saugus Formation localities. Multiple types of gneissoid and less common schistose clasts also occur. Most of the rare andesitic, felsitic, and sedimentary clasts are probably recycled from Paleocene conglomerates. Clasts sourced from the metaplutonic Mount Lowe intrusive suite and the anorthosite-syenite complex range between common and absent amidst the usually dominant other rock types.

Multiple petrofacies of the marginal zone of the Mount Lowe intrusive suite are present as clasts. Represented are the hornblende facies (abundant hornblende metacrysts and accessory sphene notable), hornblende-K-feldspar facies (ovoid feldspar and widely spaced black hornblende metacrysts notable), and hornblende-K-feldspar-garnet facies (large K-feldspar and garnet metacrysts, and biotite notable) (Ehlig, 1975a, Smith, 1986, p. 9; Barth and Ehlig, 1988, p. 193-194). Clasts from the hornblende-K-feldspar facies might be the most abundant. Clasts of the Paleoproterozoic gneiss suite are widespread in the study area but may be most abundant in the northwest sector. Massive plutonite clasts may be most abundant in the Gold Canyon-Gold Canyon Saddle area. Saugus Formation exposures on some areas of private property are not accessible.

Table 2. Maximum size, shape, and relative abundance of clasts in the Saugus Formation that are identifiable as derived from the Mount Lowe intrusive suite and anorthosite-syenite complex at 63 Saugus Formation exposures between Pacoima Wash and Gold Canyon.

[Included are maximum dimension of all clast types and summary lithologic description at each locality. Clast sizes and localities are shown in figure 10. AN = anorthosite-syenite complex clasts, ML = Mount Lowe intrusive complex clasts, N = none observed; R = rounded, SR = subrounded, SA = subangular, A = angular, NM = no measurements; * = Mount Lowe intrusive suite clasts with microcline phenocrysts; # = Mount Lowe intrusive suite clasts with garnet phenocrysts; ? = limited exposure or number of clasts: larger clasts possible or ML/AN ratio uncertain.]

Map symbol	Maximum clast dimension (cm) and shape			Relative abundance of ML and AN	Remarks
	Mount Lowe intrusive suite (ML)	Anorthosite-syenite complex (AN)	All clast types		
Westward from upper Gold Canyon and east and south of the Lopez Fault					
1	≥5? SR	≥13? SR	≥48?	AN>ML?	Sandstone, coarse-grained, pebbles-cobbles, rare boulders. Limited outcrop, poor exposure.
2	51* SR	33 SR	90	AN>ML	Conglomerate, poorly stratified, cobbles-boulders, with sandstone interbeds, massive, coarse-grained. Sequence overlies Gold Canyon beds and is stratigraphically lower than localities 3 through 5.
3	36 SR	48 SR	100	AN>ML	Sandstone, massive, coarse-grained, and conglomerate, cobbles-boulders, beds ≥ 2 m thick.
4	25 SR	30 R-SR	107	AN>ML	Sandstone, massive, coarse-grained, with conglomerate lenses, massive, boulders, and scarce red-tinted paleosol horizons.
5	46*# R-SR	46 SR-SA	86	AN=ML	Conglomerate, boulder, ,≥ 2 m thick (see fig. 9), and sandstone, coarse-grained, massive. Scarce red-tinted paleosol horizons.

Table 2. Maximum size, shape, and relative abundance of clasts in the Saugus Formation that are identifiable as derived from the Mount Lowe intrusive suite and anorthosite-syenite complex at 63 Saugus Formation exposures between Pacoima Wash and Gold Canyon—Continued.

Map symbol	Maximum clast dimension (cm) and shape			Relative abundance of ML and AN	Remarks
	Mount Lowe intrusive suite (ML)	Anorthosite-syenite complex (AN)	All clast types		
6	25* SR	36 SR	>36	AN>ML	Sandstone, massive, medium- to coarse-grained, red-tinted paleosol horizons, and pebble-boulder lenses.
7	41* SR	41 SR	112	AN>ML	Conglomerate, massive, boulders, with sandstone lenses, coarse-grained.
8	48* R-SR	53 R-SR	168	ML>AN	Conglomerate, massive, boulder, and sandstone lenses, thin, coarse-grain. Sequence rests depositionally on basement rocks.
9	30*# R-SR	71 R-SR	71	AN>>ML	Sandstone, coarse-grained, pebbles, conglomerate, cobbles-boulders, and minor red-tinted paleosol horizons. Rare magnetite-hornblende clasts from anorthosite-syenite complex.
10	25* SR	30 SR	46	AN>ML	Sandstone, coarse-grained, with pebble to boulder lenses.
11	30* SR	30 R-SR	81	AN>>ML	Conglomerate, massive, small boulders, and conglomeratic sandstone, coarse-grained.
12	48* R-SR	38 R-SR	109	AN>>ML	Conglomerate, poorly stratified, boulders, with sandstone lenses.
13	28* R	60 SR-SA	66	AN>ML	Conglomerate, massive, boulders, with rare thin sandstone lenses.
14	76* R-SR	58 SR-SA	76	AN>ML	Conglomerate, massive, boulders, with single sandstone lens, medium-grained, current laminations.
15	NM	NM	NM	AN≥ML	"...almost wholly anorthosite; very little gabbro-norite and Mendenhall Gneiss" (Weber, 1982, plate 2, locality 125).
16	23*# R-SR	51 R-SA	61	AN>ML	Sandstone, poorly stratified, coarse-grained, pebble-, and cobble-rich lenses, rare boulders; some lenses rich in Mount Lowe intrusive suite clasts, others in anorthosite clasts.
17	N	≥4? A	≥4?	AN>ML?	Sandstone, massive, coarse-grained, horizons of angular anorthosite pebbles.
18	N	≥2? A	≥2?	AN>ML?	Sandstone, masssive, coarse-grained, with red-tinted paleosol horizons, common anorthosite granules and small pebbles.
19	≥7?# SA	≥9? SR	≥28?	AN>ML?	Sandstone, massive, coarse-grained, with pebble- and small cobble-rich lenses, rare boulders; several red-tinted paleosol horizons.
20	32# R-SR	25 R-SR	51	AN>ML	Sandstone, poorly stratified, conglomeratic, mostly pebbles and cobbles, few boulders.
21	N	≥3? SA-A	30	AN	Sandstone, massive, coarse-grained, with pebble- and cobble-rich lenses, rare boulders, and thin red-tinted paleosol horizons.
22	N	25 SR	25	AN	Sandstone, poorly stratified, coarse-grained, with pebble-cobble lenses and reddish paleosol horizons. Most clasts are anorthosite and most are much smaller than the largest measured.
23	N	23 SA	23	AN	Sandstone, massive, fine- to medium-grained, red-tinted, paleosol horizons, interbedded with sandstone, massive, coarse-grained, pebbles-cobbles.
24	N	11 SR-SA	19	AN	Sandstone, massive, coarse-grained, pebble- and cobble-rich lenses, and sandstone, ≤ 1.5 m thick, fine- to medium-grained, red-tinted paleosol horizons.
25	N	10 SR-SA	23	AN	Sandstone, stratified (≤3 m thick), silty, fine- to medium-grained, red-tinted paleosol horizons, with interbedded sandstone, coarse-grained, pebbles and cobbles.
26	≥12* R-SR	NM	≥12		Sandstone, massive, coarse-grained, with pebble- and cobble-rich lenses.

Table 2. Maximum size, shape, and relative abundance of clasts in the Saugus Formation that are identifiable as derived from the Mount Lowe intrusive suite and anorthosite-syenite complex at 63 Saugus Formation exposures between Pacoima Wash and Gold Canyon—Continued.

Map symbol	Maximum clast dimension (cm) and shape			Relative abundance of ML and AN	Remarks
	Mount Lowe intrusive suite (ML)	Anorthosite-syenite complex (AN)	All clast types		
27	N	N	4		Sandstone, massive, poorly sorted, scarce pebbles, overlain by sandstone, fine- to medium-grained, red-tinted paleosol horizons.
28	8 SR	15 SR-SA	28	AN>ML	Sandstone, massive, coarse-grained, pebbles, with conglomerate lens, boulders, overlying prominent 7.5-m thick sandstone, fine- to medium-grained, red-tinted paleosol horizons.
29	36* R	33 R-SR	36	AN>ML	Sandstone, partly massive, partly cross-bedded, medium- to coarse-grained, pebbles, and conglomerate, pebbles to boulders. Several cut-and-fill channels.
30	25* SR	41 SR	41	AN>ML	Sandstone, massive, coarse-grained, pebbles, and conglomerate, pebbles to boulders.
31	25 SR	30 SR	36	AN>ML	Sandstone,conglomeratic, with conglomerate lens, irregular, pebbles to boulders.
32	23 R	36 SR	36 SR	AN>ML	Sandstone, massive, coarse-grained, pebbles, with sandstone lenses, conglomeratic, cobbles to boulders, and several red-tinted paleosol horizons.
33	10 SR	18 SR	30	AN>ML	Sandstone, poorly stratified, coarse-grained, with conglomerate lenses, pebbles to rare boulders.
34	36 SA	5 R-SR	36	ML>>AN	Sandstone, poorly stratified, medium- to coarse-grained, and sandstone, conglomeratic, cobbles to scarce boulders.
35	46* SR	61 SR	61	AN>ML	Sandstone, poorly stratified,coarse-grained, with conglomerate lens, boulders.
36	18 SA	N	28	ML	Sandstone, massive, coarse-grained, with pebble lenses and cut by pebble to cobble conglomerate-filled channels. Rare boulders.
37	10 SR	13 SR	20	AN>ML	Sandstone, poorly stratified, coarse-grained, with cobble lenses.
38	8 SR	8 SR	23	AN≈ML	Sandstone, poorly stratified, coarse-grained, with cobble lenses.
39	≥8* SR	N	≥17	ML	Sandstone, poorly stratified, medium- to coarse-grained, with pebble-rich lenses, some cobbles.
40	23 SR	N	23	ML	Sandstone, poorly stratified, medium- to coarse-grained, with pebble-rich lenses, some cobbles.
41	38* R-SR	N	38	ML	Conglomerate, cobbles, boulders, with rare thin sandstone lenses.
42	33 SR	7 SR-SA	33	AN>ML	Sandstone, poorly stratified, medium- to coarse-grained, with numerous pebble lenses, some cobbles, rare boulders.
43	≥6* SR	≥12 SR	≥12	ML>AN	Sandstone, poorly stratified, medium- to coarse-grained, pebbles, uncommon cobbles, rare small boulders.
44	13*# SR	10 R	30	ML>AN	Sandstone, moderately stratified, medium- to coarse-grained, pebbles, uncommon cobbles, rare boulders.
45	48* R-SR	23 SR	48	ML>AN	Conglomerate, poorly stratified, sandy, pebbles, cobbles, rare boulders.
46	33 R	18 SR	33	AN>ML	Sandstone, poorly stratified, coarse-grained, pebbles, rare cobbles and boulders. overlying >10-m-thick sandstone sequence, fine-grained, silty, red-tinted, paleosol horizons.

Table 2. Maximum size, shape, and relative abundance of clasts in the Saugus Formation that are identifiable as derived from the Mount Lowe intrusive suite and anorthosite-syenite complex at 63 Saugus Formation exposures between Pacoima Wash and Gold Canyon—Continued.

Map symbol	Maximum clast dimension (cm) and shape			Relative abundance of ML and AN	Remarks
	Mount Lowe intrusive suite (ML)	Anorthosite-syenite complex (AN)	All clast types		
47	15 R-SR	20 SR	>20	AN>ML	Sandstone, poorly stratified, coarse-grained, pebbles, with cobble-rich lenses.
48	≥9# SR	≥10 SR-SA	>10?	AN>ML	Sandstone, poorly stratified, coarse-grained, with pebble- and cobble-rich lenses. Unweathered Saugus Formation cobble of reddish (10R 6/2) porphyritic andesite collected near this locality.
49	≥5#	12 SR	15	AN	Sandstone, partly to poorly stratified, coarse-grained, pebbles, cobbles.
50	≥12 R-SR	≥6 SR	≥12	ML≥AN?	Sandstone, poorly stratified, medium- to coarse-grained, pebbles, with cobble-rich lenses.
North and West of Lopez Fault					
51	N	N	36		Sandstone, poorly stratified, conglomeratic, angular to subangular pebbles, cobbles, and rare boulders, with sandstone lenses, coarse-grained, and minor red-tinted paleosol horizons.
52	N	N	10		Sandstone, masssive, very poorly sorted, with scarce angular to subangular pebbles and cobbles.
53	N	N	10		Sandstone, massive, very poorly sorted, with angular to subangular pebbles and scarce cobbles.
54	N	N	25		Sandstone, poorly stratified, very poorly sorted, with abundant mostly angular to subangular pebbles and cobbles.
55	N	N	9		Sandstone, very poorly stratified, very poorly sorted, with abundant angular to subangular pebbles and cobbles.
56	N	N	7		Sandstone, massive to poorly bedded, medium- to coarse-grained, with scarce trains and thin lenses of subrounded to subangular pebbles-cobbles and red-tinted paleosol horizons.
57	N	N	8		Sandstone, massive to poorly bedded, poorly sorted, mostly angular pebbles and rare cobbles.
58	N	N	7		Sandstone, poorly bedded, poorly sorted, mostly angular pebbles, scarce cobbles.
59	N	35 SR	≥35	AN	Sandstone, conglomeratic, subangular to subrounded pebbles to boulders.
60	N	N	>10		Sandstone, silty to medium grained, red-tinted, well-formed paleosols, with sandstone interbeds, poorly sorted, mostly angular to subangular pebbles, scarce cobbles.
61	N	20 SR	≥20	AN	Sandstone, conglomeratic, mostly angular to subangular pebbles-cobbles.
62	N	N	5		Sandstone, silty to medium grained, red-tinted paleosol horizons, with sandstone lenses, coarse-grained, pebbles.
63	N	20 SR	≥20	AN	Sandstone, conglomeratic, mostly angular to subangular pebbles-cobbles.
64	N	N	5		Sandstone, coarse grained, mostly subangular to angular pebbles, and sandstone, silty to medium-grained, red-tinted paleosol horizons.

Appendix 2. Isotopic Age Determinations Using $^{87}Sr/^{86}Sr$ Ratio

The $^{87}Sr/^{86}Sr$ ratio in seawater has varied systematically through geologic time (Burke and others, 1982). Calcium-bearing minerals precipitated from seawater record this ratio. If unchanged during postprecipitation diagenesis, the ratio can be used for age determination by comparing it to a table of its variation in seawater over time. Identifying samples that have retained the original seawater ratio can be a challenge. The Neogene is a favorable time period in which to apply strontium isotope stratigraphy because seawater shows a rapid monotonic rise in $^{87}Sr/^{86}Sr$, especially during the earlier Neogene.

Originally low-Mg calcite shells are the most likely to retain the original $^{87}Sr/^{86}Sr$ ratio. In this study, translucent foliated oyster and pecten shells and, at some sites, barnacles that retain original internal structure were preferentially collected. During diagenesis, Mn and Fe increase and Ca and Sr decrease (for example, Brand and Veizer, 1980). Carbonates low in Fe and Mn and with

Table 3. Analytical results and derived $^{87}Sr/^{86}Sr$ ages of fossil samples (marine shell carbonate plus fish debris and collophane) from the Gold Canyon beds and from the late Miocene Modelo and late Miocene to early Pliocene Towsley Formations at 15 selected sites along the southwest margin of the San Gabriel Mountains and the San Fernando Pass area.

[Locations are shown in figures 2-5. Ages are assigned from the look-up table of McArthur and Howarth (2004). Fe, Mn, and Sr abundances are by ICP analysis. Analytical procedure and assessment of age reliability are discussed in Appendix 2. $\Delta sw = (^{87}Sr/^{86}Sr_{unknown} - ^{87}Sr/^{86}Sr_{modern\ seawater}) \times 105$. NBS987 = 0.710240; modern seawater = 0.709173. Qualitative judgement factors shown by plus or minus signs are based on "field" occurrence situation, fossil "quality" or suitability, "trace" element consideration in Sr analysis, and overall agreement among all analytical information. Weighted averaging of $^{87}Sr/^{86}Sr$ ratios and apparent ages in bold numerals are used to calculate "best estimate of age"; number of separate isotopic measurements are in parentheses; uncertainties partly governed by judgement factors in some cases. BFS = benthic foraminiferal stage.]

Map symbol	Latitude (N) Longitude (W) (degrees)	$^{87}Sr/^{86}Sr$	Δsw	Age (Ma)	Fe (ppm)	Mn (ppm)	Sr (ppm)	Field	Fauna	Quality	Trace	Agree
AB	34.31490 -118.28353	**0.709029±12**	**-14.4**	**5.3 ± 0.5**	**132**	**70**	**1054**	-	+	+	+	+
		0.709033±10	**-14.0**	**5.2 ± 0.4**	**103**	**141**	**1760**	+	+	+	+	+
		0.709033±13	**-14.0**	**5.2 ± 0.6**	**36**	**73**	**1259**	+	+	+	+	+
		0.709054±17	-11.9	4.1 ± 1.7	116	88	1558	+	+	+	+	+
	34.31482 -118.28261	0.709051±14	-12.2	4.4 ± 1.7	68	54	877	-	+	+	+	+
		0.709057±14	-11.6	3.8 ± 1.3	16	24	1082	+	+	+	+	+
C	34.27398 -118.30159	0.708974±16	-29.9	6.4 ± 0.4	393	1704	832	+	+	+	-	-
		0.708857±13	-32.2	11.2 ± 0.7	3005	953	3282	+	+	+	+	+
F	34.29076 -118.32632	**0.708915±15**	**-25.8**	**9.2 ± 1.4**	**733**	**254**	**805**	+	+	+	+	+
		0.708900±14	-27.3	9.7 ± 0.8	654	995	647	+	+	+	-	+
		0.708908±16	-26.5	9.4 ± 1.1	213	229	1561	-	-	-	+	+
		0.708922±17	**-25.1**	**8.8 ± 1.4**	**160**	**188**	**961**	+	+	+	+	+
		0.708891±17	-28.2	9.9 ± 0.8	1029	4035	558	+	+	+	-	+
G	34.29819 -118.33673	**0.708837±14**	**-33.6**	**12.1 ± 1.1**	**58**	**50**	**847**	+	+	+	+	±
		0.708876±11	-29.7	10.4 ± 0.5	503	813	455	+	+	+	-	±
H	34.30424 -118.33842	0.709091±14	-8.2	1.9 ± 0.4	106	365	2479	-	-	-	+	-
K	34.29272 -118.36713	**0.708916±14**	**-25.7**	**9.1 ± 1.4**	**364**	**32**	**814**	+	+	+	+	+
		0.708907±14	**-26.6**	**9.5 ± 0.9**	**135**	**27**	**547**	+	+	+	+	+
L	34.29324 -118.36715	**0.708995±10**	**-17.8**	**6.0 ± 0.2**	**104**	**336**	**850**	-	+	-	-	-
		0.708974±14	**-19.9**	**6.4 ± 0.4**	**81**	**146**	**1660**	-	-	-	+	+
		0.708962±12	**-21.1**	**6.8 ± 0.4**	**129**	**62**	**1023**	+	+	+	+	+
		0.708971±10	**-20.2**	**6.5 ± 0.3**	**390**	**690**	**750**	+	+	+	-	+

high Sr/Mn ratios are most likely to have retained original seawater ratios (Denison and others, 1994). Trace element composition of shell material is used to determine which samples are potentially reliable. As guidelines, samples having <300 ppm Mn, <3,000 ppm Fe, and Sr/Mn >2 are considered to have favorable trace elements (table 3). Less favorable shell species were analyzed from some sites, either because no better shell material was found or the extent of diagenetic exchange was sought.

Where possible, multiple shell fractions were collected and prepared for each locality. Crushed and washed shells were hand picked for analysis. A numeric age was assigned to each analyzed sample using the Look-up Table of McArthur and Howarth (2004). That table is based on curve construction using LOWESS fitting of isotopic analyses and stratigraphic assignments (Howarth and McArthur, 1997; McArthur and others, 2001). The Neogene part of the curve and Look-up Table is based largely on data from Deep Sea Drilling Project and Ocean Drilling Program sites. More details of strontium separation and isotopic analysis are described in McCulloh and others (2002).

The precision of the numeric age assigned to individual isotopic analyses in table 3 depends on the measurement error of the isotope ratio, the error band in the reference seawater curve, and the slope of the reference curve. The overall reliability of each analyzed sample is judged from the clarity of field relations, fossil quality ("fauna" column), trace-element content, and the agreement among analyses from the locality (table 3). Ultimately the isotopic agreement from shell material judged most reliable is the sole criterion of a retained ratio and therefore a meaningful age.

Table 3. Analytical results and derived $^{87}Sr/^{86}Sr$ ages of fossil samples (marine shell carbonate plus fish debris and collophane) from the Gold Canyon beds and fom the late Miocene Modelo and late Miocene to early Pliocene Towsley Formations at 15 selected sites along the southwest margin of the San Gabriel Mountains and the San Fernando Pass area—Continued.

Best estimate of age ($^{87}Sr/^{86}Sr$) (Ma)	Fossil material used	Remarks
0.709032 ± 2 (3) **5.2 ± 0.3** 0.709043 ± 12 (6) 4.2 ± 1.3	Oyster, grey, translucent, foliated fragments	Isotopic ratios, from a suite of excellent samples with favorable trace elements, equivalent to basal Pliocene seawater.
	Pectinid, pinkish, foliated fragements	
	Oyster, white to pale pinkish, foliated fragments	
	Oyster, thin, white, translucent, foliated fragments	
	Oyster, thin, white, translucent, foliated fragments	
	Oyster, white, translucent, foliated fragments	
anomalous ages	Oyster spat	Modelo Fm. In silty diatomaceous and foraminiferal claystone (see Appendixes 3-5). Inconsistency between Mn/Sr ratios and apparent ages indicates altered Sr.
	Fish debris (scales and bones).	
0.708919 ± 5 (2) **9.0 ± 0.6** 0.708911 ± 9 (5) 9.3 ± 0.7	Oyster, thin, tan, foliated fragments	Correlative with late Mohnian BFS part of Modelo Formation (Barron and Isaacs, 2001, p. 294). Mapped as Monterey Fm. by Dibblee (1991b). Consistent results from samples of variable quality suggests a reliable age, but divergence from age based on calcareous nannofossils and diatoms, from nearby overlying strata (locality U), indicates this age is apparently young by about 1 Ma or more. One or both age calibrations may be in error. Disparity does not affect our structural interpretation.
	Pectinid, grey to tan foliated fragments	
	Bivalve, white, chalky	
	Oyster, white, tranlucent, foliated fragments	
	Oyster, pink, blocky, fibrous fragments	
0.708837 ± 14 (1) **12.1 ± 1.1**	Pectinid, white, foliated fragments	Equivalent to early Mohnian BFS part of Modelo Fm. on basis of Sr isotopic age. Mapped as Monterey Fm. by Dibblee (1991b). Better sample yields preferred age.
	Oyster, pinkish, blocky, fibrous fragments	
anomalous age	Bivalve, thin, white, chalky fragments	Monterey (?) Formation of Dibblee (1991b). Undesirable fossil type with altered shells.
0.708912 ± 14 (2) **9.3 ± 1.1**	Oyster spat	Correlative with oldest part of late Mohnian BFS and therefore Modelo Formation (see appendixes 3 and 4).
	Oyster spat	
0.708976 ± 13 (4) **6.3 ± 0.3**	Pectinid, white to pinkish, partly opaque, foliated fragments	Lower Delmontian BFS equivalent and therefore correlative of Towsley Formation. Consistent results from samples of variable quality indicates a reliable age.
	Bivalve, white chalky fragments	
	Pectinid, large ribbed, grey, foliated shell	
	Pectinid, thin, gray, foliated shell	

Table 3. Analytical results and derived $^{87}Sr/^{86}Sr$ ages of fossil samples (marine shell carbonate plus fish debris and collophane) from the Gold Canyon beds and from the late Miocene Modelo and late Miocene to early Pliocene Towsley Formations at 15 selected sites along the southwest margin of the San Gabriel Mountains and the San Fernando Pass area—Continued.

Map symbol	Latitude (N) Longitude (W) (degrees)	$^{87}Sr/^{86}Sr$	Δsw	Age (Ma)	Fe (ppm)	Mn (ppm)	Sr (ppm)	Field	Fauna	Quality	Trace	Agree
M	34.29348 -118.40030	**0.709011±7**	**-16.2**	**5.7 ± 0.2**	**2326**	**873**	**2074**	+	?	?	-	+
		0.709016±15	**-15.7**	**5.6 ± 0.5**	**1323**	**804**	**1620**	+	?	?	-	+
N	34.30132 -118.40858	**0.709068±17**	**-10.5**	**2.7 ± 0.8**	**328**	**125**	**911**	-	+	+	+	+
		0.709071±13	**-10.1**	**2.5 ± 0.6**	**92**	**41**	**805**	-	+	+	+	+
		0.708989±17	-18.4	6.1 ± 0.3	718	241	910	-	+	+	+	-
		0.709077±16	**-9.6**	**2.3 ± 0.6**	**163**	**58**	**890**	-	+	+	+	+
		0.709055±14	**-11.8**	**4.0 ± 1.5**	**27**	**107**	**785**	-	+	+	+	+
		0.709052±15	**-12.1**	**4.3 ± 1.7**	**62**	**31**	**987**	-	+	+	+	+
		0.709027±13	-14.6	5.3 ± 0.5	21	10	1941	-	-	-	+	+
		0.709060±8	-11.3	3.4 ± 0.8	14	5	2193	-	-	-	+	+
P	34.33443 -118.45564	**0.709015±11**	**-15.8**	**5.7 ± 0.4**	**1108**	**73**	**797**	+	+	+	+	+
	34.33705 -118.45602	**0.708991±15**	**-18.2**	**6.1 ± 0.3**	**45**	**12**	**992**	+	+	+	+	+
R	34.33207 -118.45632	0.708933±13	-24.0	8.2 ± 1.0	1950	611	519	-	-	-	-	-
		0.708881±14	-29.2	10.2 ± 0.6	151	74	1140	+	+	-	+	-
T	34.32783 -118.48837	0.708775±18	-39.8	15.2 ± 0.7	288	200	778	-	+	+	+	±
		0.707727±17	-144.6	anomalous	458	270	485	-	+	-	-	-
		0.708762±19	-41.1	15.4 ± 0.5	316	122	707	-	+	+	+	±
		0.708663±19	-51.0	17.0 ± 0.4	210	125	554	-	+	+	+	-
U	34.35936 -118.49896	**0.708966±9**	**-20.7**	**6.7 ± 0.3**	**211**	**69**	**1100**	+	+	+	+	+
		0.708982±9	**-19.7**	**6.2 ± 0.2**	**531**	**180**	**553**	+	-	+	+	+
W	34.34866 -118.52919	0.708882±9	-29.1	10.2 ± 0.4	48	66	1590	-	-	+	+	±
		0.708848±15	-32.5	11.4 ± 0.8	81	37	2640	-	-	+	+	±
		0.708742±10	-43.1	15.7 ± 0.3	98	484	806	-	-	-	-	-
X	34.36063 -118.55739	**0.709010±9**	**-16.3**	**5.8 ± 0.3**	**170**	**45**	**810**	+	+	+	+	+
		0.709025±15	**-14.8**	**5.4 ± 0.6**	**259**	**59**	**821**	+	+	+	+	+
		0.709027±14	**-14.6**	**5.3 ± 0.5**	**254**	**72**	**802**	+	+	+	+	+

Table 3. Analytical results and derived $^{87}Sr/^{86}Sr$ ages of fossil samples (marine shell carbonate plus fish debris and collophane) from the Gold Canyon beds and fom the late Miocene Modelo and late Miocene to early Pliocene Towsley Formations at 15 selected sites along the southwest margin of the San Gabriel Mountains and the San Fernando Pass area—Continued.

Best estimate of age ($^{87}Sr/^{86}Sr$) (Ma)	Fossil material used	Remarks
0.709014 ± 1.0 (2) 5.7 ± 0.2	Fish bone and phosphatic matrix from coprolite	Towsley Formation equivalent. Experience with Sr isotopic dating of phosphatic material is limited, but late Delmontian BFS is reasonable.
	Phosphatic matrix from same coprolite	
0.709065 ± 11 (5) 2.7 ± 0.5 0.709059 ± 16 (7) 2.9 ± 0.6	Pectinid fragments, handpicked	Mapped as an uppermost part of the Towsley Formation of Dibblee (1991a), it is possible these strata correlate to the Sunshine Ranch Member of the Saugus Formation (Winterer and Durham, 1962, plate 44, and text). Five pectinids with the most favorable trace elements yield consistent results.
	Pectinid, deeply ribbed, foliated fragment	
	Pectinid. foliated fragment	
	Pectinid, foliated fragement	
	Pectinid, foliated fragment	
	Pectinid. foliated fragment	
	Bivalve (?), vitreous exterior with dense, brown interior	
	Bivalve (?), dense, brown fragment	
0.709003 ± 17 (2) 5.9 ± 0.4	Barnacle, resinous translucent fragments	Basal Towsley Formation resting on basement. Correlative of middle Delmontian BFS based on Sr isotopic age.
	Pectinid, white to pinkish, translucent, foliated fragments	
anomalous ages	Mollusk, thin, white , partly chalky fragments	Basal Towsley Formation. Inconsistency between Mn/Sr ratios and apparent ages indicates altered Sr (see Appendix 2).
	Barnacle, pinkish, dense fragments	
anomalous ages	Pectinid, white to pinkish, ribbed, foliated fragments	From vertical strata beneath the north-dipping Santa Susana Fault. Strongly anomalous result for barnacle suggests all ages are anomalous.
	Barnacle, pink, unstructured fragments	
	Oyster, mostly foliated	
	Oyster, mostly foliated	
0.708974 ± 11 (2) 6.4 ± 0.3	Pectinid, tan, translucent, foliated fragment	Towsley Formation in Elsmere Canyon. Correlative with Delmontian BFS.
	Bivalve, brownish, resinous, translucent fragment	
anomalous ages	Bivalve, thin, pinkish, vitreous fragments	Pico Formation of Winterer and Durham (1962, plate 44) closely correlative with 5 Ma horizon. First two apparent ages judged unreliable due to aragonitic shells or occurrence in possibly recylced fossil-bearing clasts? Third apparent age unreliable because of Mn/Sr ratio.
	Gastropod, vitreous, some with chalky patina	
	Mollusk, uncertain origin, grey foliated fragments	
0.709021 ± 9 (3) 5.5 ± 0.4	Oyster, mostly translucent and foliated fragments	Top of Pico Formation of Winterer and Durham (1962, plate 44). Correlative with the late Delmontian BFS.
	Oyster, translucent, foliated fragments	
	Oyster, transparent, foliated fragments	

Appendix 3. Identification, Age, and Paleoenvironment of Calcareous Nannofossils

Calcareous nannofossils were recovered from geographically and stratigraphically separated outcrops south and southeast of the Merrick Syncline (localities K and C on fig. 2*B*) and on its northeast flank (locality E on fig. 2*B*). These floras provide information about stratigraphic position, age range, and correlation to more fossiliferous and better studied sections, as well as giving hints about the paleooceanographic conditions when these phytoplankton communities lived.

Nannofossil assemblages from localities K and C allow assignment to the CN 7b-CN 8a zones (Okada and Bukry, 1980; Young, 1998) that straddle the lower-upper Mohnian BFS boundary (Blake, 1991) and indicate an age between 9.8 and 8.8 Ma (Fornaciari, 2000, table 6; Backman and Raffi, 1997, table 1; respectively) (table 4). This age range for locality K brackets the 9.3±1.1 Ma age determined by $^{87}Sr/^{86}Sr$ analyses (appendix 2, table 3, appendix 4). For locality C, a 9.8 to 8.8 Ma age range indicated by calcareous nannofossils is consistent with the Mohnian BFS assignment based on benthic foraminifers (appendix 4, table 5) and with the 9.5 to 9.2 Ma assignment from diatom data (appendix 5, table 6), but it is younger than the 11.2 ±0.7 Ma age from $^{87}Sr/^{86}Sr$ analyses (appendix 2, table 3).

All samples from locality E yield nannofossils that are calcareous nannofossil zone CN 5a or younger (Okada and Bukry, 1980; Theodoridis, 1984; Young, 1998) (table 4). Assemblages in samples E-1 and E-1B are restricted to CN 5 (Okada and Bukry, 1980; Young, 1998), but E-2 and E-4 may be as young as CN 7 (Okada and Bukry, 1980; Perch-Nielsen, 1985; Young, 1998). This evidence places all four samples in the lower Mohnian BFS (Blake, 1991) and indicates a maximum age of 13.53 Ma and a minimum age of 10.9 Ma (E-1 and E-1B) to 9.67 Ma (E-2 and E-4) (Lourens and others, 2004, table A2.2). These results are consistent with, but better constrained by, the 12.3 to 11.5 Ma assignment of sample E-2 based on diatom data (appendix 5, table 6).

Phytoplankton from locality C are typical of well-mixed high nutrient upwelling based on abundant diatoms and rare nannofossils (Margalef, 1978) and on the high abundance of *Reticulofenestra pseudoumbilicus* (>5 μm) (Flores and others, 2005). All sites yield rare warm-water, oligotrophic species of *Discoaster* and *Sphenolithus* and one or more abundant mesotrophic and/or eutrophic species: *Reticulofenestra pseudoumbilicus* (<5 μm), *Reticulofenestra pseudoumbilicus* (>5 μm), and *Coccolithus pelagicus* (Flores and others, 2005). These assemblages suggest various phases of upwelling, even though abundant oyster spat at localities K and C (appendix 4) indicate deposition very close to the paleoshoreline.

Table 4. Calcareous nannofossils identified in Modelo Formation outcrop samples at three localities from Little Tujunga Canyon to near the mouth of Big Tujunga Canyon.

[See figure 2*B* for localities. Correlation of California benthic foraminiferal stages to Okada & Bukry (1980) calcareous nannofossil zones are after Blake (1991). Nannofossil ranges are from Young (1998) except for the ranges of *Helicosphaera minuta* and *Syracosphaera fragilis,* which are based on Perch-Nielson (1985) and Theodoridis (1984), respectively. The "Taxa abundance by locality" section reports the actual number of each species counted per sample. Below this section are statistics and comments about each sample. These statistics include "Nannofossils per mm^2" which normalizes the abundance of all fossils per slide to show the wide range of their abundance. VR = very rare.]

Age-diagnostic and associated taxa	California benthic foraminiferal stages										Taxa abundance by locality					
	Luisian	Mohnian								Del-montian	Map symbol					
		Lower					Upper									
	CN Zones										E-1	E-1B	E-2	E-4	K	C
	4	5a	5b	6	7a	7b	8a	8b	9a	9b						
Braarudosphaera bigelowii												VR	4			
Calcidiscus leptoporus											VR	8	VR	4	10	11
C. tropicus												3		3		3
Coccolithus miopelagicus (>14 μm)	<	X	X									VR				
C. pelagicus pelagicus											2	49	1	48	243	91
Coronocyclus nitescens												VR				
Cyclicargolithus floridanus	<	X	IN[1]								VR					
Dictyococcites antarcticus											14	16	4	65		17
D. productus											89	744	341	81	21	24
Discoaster exilis	<	X	X	X	X	X						1	VR	3		

Table 4. Calcareous nannofossils identified in Modelo Formation outcrop samples at three localities from Little Tujunga Canyon to near the mouth of Big Tujunga Canyon—Continued.

Age-diagnostic and associated taxa	California benthic foraminiferal stages										Taxa abundance by locality					
	Luisian	Mohnian								Del-montian	Map symbol					
		Lower						Upper								
	CN Zones										E-1	E-1B	E-2	E-4	K	C
	4	5a	5b	6	7a	7b	8a	8b	9a	9b						
D. sp. cf. *D. exilis*														VR	5	3
D. intercalaris															1	
D. spp.												VR		VR	11	1
D. variabilis															1	
Helicosphaera carteri												VR	VR	1	11	1
H. intermedia												VR		VR		
H. minuta	X	X	X	X	X	X							7	10		
Lithostromation perdurum												6	1	VR		1
Minylitha convallis						X	X	X	IN[1]						6	1
placoliths (unidentifiable species)											13	VR	VR	17	33	61
Pontosphaera discopora												VR		VR		
P. multipora														VR		
Reticulofenestra minuta											12	6,231	2,397	24	2	4
R. minutula											13	991	623	201	27	39
R. pseudoumbilica (5-7 µm)	<	X	X	X	X	X	X			>	53	544	141	207	71	212
R. pseudoumbilica (>7 µm)		IN[1]	X	X	X	X	X			>	117	37	1	46	68	200
Rhabdosphaera pannonica													5			
R. sp.													4	VR		
Sphenolithus neoabies											4	6	1	19	8	7
Syracosphaera fragilis		X	X	X	X	X	X	X		X			6			
Triorbis sp.												VR	VR			
Triquetrorhabdulus sp. cf. *T. rugosus*															3	1
T. sp. cf. *T. rioi*											VR	VR	VR	VR		
Umbilicosphaera sibogae foliosa																1
General Preservation (P-Poor, M-Moderate, G-Good, E-Excellent)											M	E	E	G	M	M
Nannofossils counted											317	8,636	3,536	729	521	678
Nannofossils per mm^2											15	8,636	3,536	209	2	3
Identifiable nannofossils counted (excludes unidentifiable species)											304	8,636	3,536	712	477	616
Species identified											8	12	14	9	14	16
Fisher alpha index											1.5	1.9	1.4	1.5	2.7	3.0
CN zones represented											5a-5b	5a-5b	5-7	5-7	7b-8a	7b-8a
diatom fragments per mm^2											1	33	376	170	1	400

[1] Either the first or last occurrence of the species is within the zone.

Appendix 4. Identification, Age, and Paleoenvironment of Foraminifers and Occurrences of Fossil Oyster Spat

Foraminifers (benthic and planktonic) were identified from stratigraphically separate outcrop localities K, J, and C on the south flank, and locality E on the northeast flank, of the Merrick Syncline (fig 2*B*). Fossil species identified are shown in table 5, together with zonal assignments (Blake, 1991), age ranges for each species (Barron and Isaacs, 2001, Finger, 1990), and paleoenvironments (Finger, 1990). The unexpected discovery of fossil oyster spat associated with deep-water benthic foraminifers, an association apparently not previously described in the literature, suggests close proximity of shallow coastal marine waters to upper bathyal environments. Oyster spat from locality K were analyzed for $^{87}Sr/^{86}Sr$ age (appendix 2).

On the Merrick Syncline south flank, the stratigraphically highest sample (locality K) cannot be younger than 5.1 Ma (Delmontian BFS), based on the presence of *Uvigerina hannai*, but it probably is older (Mohnian BFS). The age range of the next stratigraphically lower sample (locality J) is 13.5 to 7.1 Ma (Mohnian BFS) based on the co-occurrence of *Gyroidina rosaformis* and *Bolivina sinuata*. The age of the stratigraphically lowest sample (locality C) is also 13.5 to 7.1 Ma based on the occurrence of *Galliherina uvigerinaformis* and its stratigraphic position below locality J. The locality C sample probably is no younger than 9.4 Ma. Traditionally, *G. uvigerinaformis* has been restricted to the early Mohnian BFS (13.5 to 9.4 Ma), but Finger (1990) extended its range to include all of the Mohnian BFS and Delmontian BFS (13.5 to 5.1 Ma). On the Merrick Syncline northeast flank, the age of samples from locality E is Mohnian based on the co-occurrence of *Galliherina uvigerinaformis, Bolivina churchi*, and *B. wissleri.*

Table 5. Abundance, zone ranges, and suggested paleoenvironments of foraminifers from four Modelo Formation outcrop localities in the area from Little Tujunga Canyon to the mouth of Big Tujunga Canyon, California.

[See figure 2*B* for sample localities. VR = very rare, R = rare, F = few, C = common, A = abundant, Flood = very numerous. Includes abundances of fish debris and oyster spat.]

Taxa	Taxa abundance by locality (map symbol; N latitude, W longitude, decimal degrees)						Benthic Foraminiferal Stage BFS or age range (Finger, 1990)	Paleoenvironment (Finger,1990)
	K 34.29272 -118.36713	J 34.29049 -118.36678	C 34.27398 -118.30159	E 34.28663 -118.31965				
				E-1	E-2	E-3		
Benthic Foraminifera								
Ammobaculites? sp.		F						marsh
Bolivina advena			R				Saucesian-Holocene	u. bathyal; O_2 minimum
B. churchi				C	F	R	Saucesian-Mohnian	
B. foraminata	F	R			F	R	Saucesian-Pliocene	u. mid. bathyal; O_2 minimum
B. cf. *B. hughesi*			VR					
B. imbricata			VR				Saucesian-Holocene	u. mid. bathyal
B. seminuda			C					u. mid. bathyal; O_2 minimum
B. sinuata		VR					Mohnian-Pliocene	u. bathyal
B. cf. *B. spissa*	F							
B. wissleri					F		Mohnian	
Bulimina cf. *B. ovata*				R				
Buliminella curta				C	C		Zemorrian-Pliocene	outer shelf; O_2 minimum
Buliminella subfusiformis				C	C		Zemorrian-Pliocene	u. bathyal; O_2 minimum
Buliminella spp.			F					
Galliherina (Bulimina) uvigerinaformis			C	F			Mohnian-Delmontian	u. mid. bathyal

Concurrent age ranges of microfossils (diatoms, calcareous nannofossils, and foraminifers) and a strontium isotope age indicate a latest early Mohnian BFS to early late Mohnian BFS age range (9.8 to 8.8 Ma) for all three south-flank samples. The stratigraphically highest sample (locality K) is no younger than early late Mohnian BFS (8.8 Ma), and the age of the stratigraphically lowest sample (locality C) is no younger than earliest late Mohnian BFS (9.2 Ma) and no older than latest early Mohnian BFS (9.9 Ma). The age of the middle sample (locality J) may be at or near the boundary between late and early Mohnian BFS (9.4 Ma). Concurrent age ranges of diatoms and calcareous nannofossils from sample E on the northeast flank indicate a middle early Mohnian BFS age range (12.3 to 11.5 Ma).

Benthic foraminifers from all samples indicate an upper bathyal to upper middle bathyal depositional depth, probably in or near the O_2 minimum zone. The presence of pelagic open-ocean microfossils (planktic foraminifers, calcareous nannofossils, diatoms, and fish debris) in samples from localities C and E indicates open-ocean and possible upwelling conditions. The presence of calcareous nannofossils and fish debris in the locality K sample also indicates open-ocean conditions. The large number of oyster spat associated with deep open-water microfossils and fish debris in samples C and K suggest close proximity of a shallow coastal environment. The lack of shallow-water foraminifers suggests that the oyster spat came from the overlying water column rather than by downslope sediment transportation.

Spat is a term used here to include all the stages of shelled pelagic oyster larvae before attachment to a substrate. Because precise biological names for the various pelagic stages are based on soft-part development rather than shell size, the use of various stage names for fossil shell material is not possible. Spat shell length in modern oysters increases with stage development but shows much variation between oyster species. Modern spat usually range from 60 μ to 300 μ in length. Fossil spat from both localities C and K range in length from 55 μ to 100 μ. Modern oyster larvae develop in 10-25 days, during which time water currents can transport them as far as 8 km from spawning grounds (Lorio and Malone 1994). The pelagic larvae have a limited ability for vertical movement, but cooling water conditions and turbidity can delay settling for as much as ten days (Lorio and Malone, 1994).

Table 5. Abundance, zone ranges, and suggested paleoenvironments of foraminifers from four Modelo Formation outcrop localities in the area from Little Tujunga Canyon to the mouth of Big Tujunga Canyon, California—Continued.

Taxa	Taxa abundance by locality (map symbol; N latitude, W longitude, decimal degrees)						Benthic Foraminiferal Stage BFS or age range (Finger, 1990)	Paleoenvironment (Finger,1990)
	K 34.29272 -118.36713	J 34.29049 -118.36678	C 34.27398 -118.30159	E 34.28663 -118.31965				
				E-1	E-2	E-3		
Gyroidina rosaformis		R					Zemorrian-Mohnian	u. mid. bathyal
Hansenica cf. *H. rotundimargo*			R					
Holmanella (Planulina) baggi		VR					Saucesian-Pliocene	outer shelf
Praeglobobulimina ? sp.		VR		C[1]	C[1]	C[1]		u. mid. bathyal; O_2 minimum
Uvigerina hannai	R						Saucesian-Delmontian	u. mid. bathyal
U. hootsi		VR					Saucesian-Pliocene	u. mid. bathyal
U. cf. *U. subperigrina*		R						u. mid. bathyal; O_2 minimum
U. sp. (broken)						VR		
Planktic Foraminifera								
Globigerina bulloides			F	F	F	R	Zemorrian-Plio/Holocene	temperate waters
G. sp.			F					
Other								
fish debris	F		A	A	A	R		
oyster spat	A		Flood					tidal

[1] Unwashed material from E-1, E-2, and E-3 contain numerous thin-shelled foraminifers on bedding planes that probably are *Praeglobobulimina* sp.

Appendix 5. Identification and Zonation of Diatoms

Well-preserved diatom assemblages were encountered in samples from locality C near the mouth of Big Tujunga Canyon and from locality E on the northeast flank of the Merrick Syncline (fig. 2*B*). The locality C assemblage is correlated with the upper part of Subzone d of the *Denticulopsis hustedtii-D. lauta* Zone (9.5-9.2 Ma), and the locality E assemblage is correlated with the lower part of Subzone c of the *Denticulopsis hustedtii-D*. lauta Zone (12.3-11.5 Ma) (Barron, 1981, 1986a) (table 6). The locality C assemblage also contains the silicoflagellate *Distephanus pseudofibula*, that ranges from ~9.5 to 7.8 Ma. According to Barron and Isaacs (2001) and Barron (2003), the locality C assemblage is correlative with earliest late Mohnian BFS and the locality E assemblage is correlative with early Mohnian BFS, the latter being older than all other diatom-bearing San Fernando Valley assemblages studied by Barron, which do not range below Subzone d of the *D. hustedii-D. lauta* Zone. Interestingly, the locality E assemblage immediately predates a compressed interval within the middle and upper parts of Subzone c of the *D. hustedtii-D. lauta* Zone that occurs in numerous coastal sections of southern California and in offshore DSDP sections. Barron (1986b) cites papers by Hoskins and Griffiths (1971) and Crouch (1979) that relate this compressed interval to uplift of the southern California continental borderland. It also appears that this compressed interval coincides with the final phase in tectonic rotation of the Santa Ynez Range (Hornafius and others, 1986).

Table 6. Diatom species and abundance from two Modelo Formation outcrop samples.

[See figure 2*B* for localities.]

Locality	**C**	**E**	
Zone, subzone	*D. hustedtii-D. lauta* subzone d	*D. hustedtii-D. lauta* subzone c	
Assemblage age range (Ma)	9.5-9.2	12.3-11.5	
Species	**Abundance**		**Taxon age range (Ma)**
Actinocyclus ingens	rare	common	18.4 - 7.7
Azpeitia cf. *nodulifera*	rare		13.3 - 0
Azpeitia cf. *vetustissima*	rare	rare	~14 - 0
Denticulopsis dimorpha	rare		9.9 - 9.2
D. praekatayamae	rare		9.5 - 8.6
D. lauta	rare	rare	15.1 - 9
D. praedimorpha	very rare (reworked)	abundant	12.4 - 11.5
D. simonsenii	abundant	abundant	13.1 - 8.6
Hemidiscus cuneiformis	rare		11.5 - 0
Nitzschia praereinholdii		rare	12.2 - 7.6
Proboscia barboi	rare	rare	12.3 - 0.3
Thalassiosira brunii	rare		12.2 - 8.9
T. cf. *flexuosa*		rare	13.6 - 9.0

Appendix 6. Age of Basalt by $^{40}Ar/^{39}Ar$ Incremental-Heating Analysis

A Topanga Group volcanic sample from locality D (fig. 2*B*), dated by $^{40}Ar/^{39}Ar$ analysis, is a partly altered, porphyritic basaltic andesite or basalt with fine-grained groundmass. Phenocrysts of altered olivine (largely opaque), clinopyroxene, and plagioclase are contained in a partly altered matrix of plagioclase microlites, clinopyroxene, and magnetite, with hematite, iddingsite, chlorite, and minor glass, some altered to clays. Plagioclase phenocrysts range from <500 μm to more than 1 mm in size, some with corroded and embayed margins. Reacted rims appear to be entirely products of magmatic reaction with the melt, and no significant alteration of these phenocrysts is noted. These phenocrysts are zoned and range in composition from about An30 to An60. The mean K_2O content of the plagioclase derived from Ar-Ar analysis is 0.28 percent. The minimum dimension of groundmass plagioclase laths averages about 10 μm, with no visible alteration.

Plagioclase from the sample was analyzed by the $^{40}Ar/^{39}Ar$ (Ar-Ar) dating technique (Merrihue and Turner, 1966). Separated 0.25 to 0.5 mm phenocrysts were irradiated with fast neutrons for 16 hours at about 1 MW power in the U.S. Geological Survey (USGS) TRIGA Reactor Facility in Denver, Colorado. USGS standard sanidine from the Taylor Creek Rhyolite (TCR-2), with an age of 27.87 Ma, was used as the flux monitor. This age is standardized to the Menlo Park intralaboratory standard biotite, SB-3, and to interlaboratory standard hornblende, MMhb1 (Samson and Alexander,

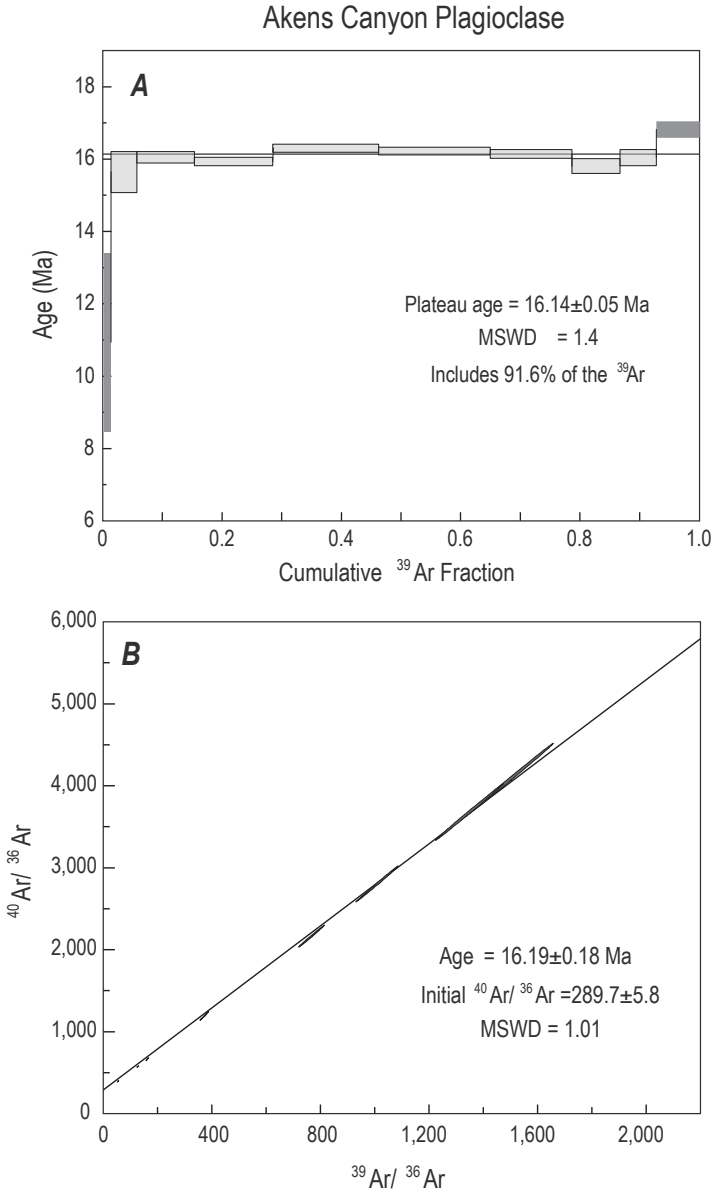

Figure 11. $^{40}Ar/^{39}Ar$ age-spectrum (*A*) and isochron (*B*) diagrams for the Topanga Group basalt sample (locality D, fig. 2*B*). The statistically uniform ages obtained from the 625°C through 1,150°C steps defines an age plateau representative of the age of the basalt.

1987) with an average age of 513.9 Ma. Decay and abundance constants for K and Ar isotopes are those recommended by Steiger and Jager (1977).

Argon was released by incremental heating of the sample from 550° to 1,300°C. Analytical errors in $^{40}Ar/^{39}Ar$ ages are reported at the 1σ level. The $^{40}Ar/^{39}Ar$ plateau age identified in the age spectrum diagram (fig. 11) represents more than 50 percent of the ^{39}Ar released and is defined as the weighted mean age of contiguous gas fractions for which no difference in age can be detected at the 95-percent level of confidence (Fleck and others, 1977). Analytical results are summarized in table 7. The $^{40}Ar/^{39}Ar$ incremental-heating data define a "plateau-type" age spectrum with an age of 16.14±0.05 Ma that represents the age of eruption and cooling of the lava (fig. 11*A*). An isochron diagram of the plateau-age steps yields an age of 16.19±0.18 Ma and MSWD of 1.01 (fig 11*B)*, confirming the plateau age and the agreement between estimated analytical error and the dispersion of data about the isochron (McIntyre and others, 1966).

Table 7.—Results of Ar-Ar analyses of plagioclase from basaltic andesite of the Topanga Group.

[See locality D on figure 2*B*. Sample designation—Akens Canyon; irradiated in the USGS TRIGA reactor, Denver, CO, as USGS Menlo Park irradiation number IRR228-51; the measure of neutron flux is J = 0.003603159. Ar_K, potassium-derived argon; Ar*, radiogenic. MSWD is mean square of weighted deviates, after McIntyre and others, 1966.]

Step (°C)	% $^{39}Ar_K$	% ^{40}Ar*	$^{40}Ar/^{39}Ar$	$^{37}Ar/^{39}Ar$	$^{36}Ar/^{39}Ar$	K/Ca	Cl/K	Age (Ma)
550	1.06	4.91	34.1136	15.7293	0.1141	0.033	0.1123	10.976 ± 2.470
625	4.46	29.74	8.0452	17.3708	0.0239	0.030	0.0211	15.665 ± 0.567
700	9.54	75.57	3.2456	18.3893	0.0077	0.028	0.0058	16.069 ± 0.157
775	13.25	86.21	2.8239	18.5167	0.0064	0.028	0.0019	15.951 ± 0.117
850	17.76	92.44	2.6928	19.7914	0.0061	0.026	0.0020	16.322 ± 0.109
925	18.84	91.69	2.6997	20.3716	0.0063	0.025	0.0041	16.238 ± 0.105
1000	13.51	89.22	2.7645	18.7637	0.0061	0.028	0.0061	16.162 ± 0.115
1075	8.14	50.96	4.7582	12.8595	0.0114	0.040	0.2699	15.829 ± 0.205
1150	6.14	57.32	4.2978	10.7282	0.0091	0.049	0.0125	16.055 ± 0.225
1300	7.30	46.49	5.5459	13.2960	0.0137	0.039	0.0063	16.828 ± 0.225
					Weighted Mean Plateau age (Ma)			16.14 ± 0.05
					Isochron age (Ma) (MSWD=1.01)			16.19 ± 0.18
					Total gas age (Ma)			16.106 ± 0.058

Produced in the Western Region, Menlo Park, California
Manuscript approved for publication, November 3, 2008
Text edited by Peter H. Stauffer
Layout and Design by Jeanne S. DiLeo


ISBN 1-4113-2330-0
9 781411 323308